

Efficient Multi-order Gated Aggregation Network

Siyuan Li^{1,2*} Zedong Wang^{1*} Zicheng Liu^{1,2} Cheng Tan^{1,2}
 Haitao Lin^{1,2} Di Wu^{1,2} Zhiyuan Chen¹ Jiangbin Zheng^{1,2} Stan.Z.Li^{1†}
¹AI Division, School of Engineering, Westlake University ²Zhejiang University

Abstract

Since the recent success of Vision Transformers (ViTs), explorations toward transformer-style architectures have triggered the resurgence of modern ConvNets. In this work, we explore the representation ability of DNNs through the lens of interaction complexities. We empirically show that interaction complexity is an overlooked but essential indicator for visual recognition. Accordingly, a new family of efficient ConvNets, named MogaNet, is presented to pursue informative context mining in pure ConvNet-based models, with preferable complexity-performance trade-offs. In MogaNet, interactions across multiple complexities are facilitated and contextualized by leveraging two specially designed aggregation blocks in both spatial and channel interaction spaces. Extensive studies are conducted on ImageNet classification, COCO object detection, and ADE20K semantic segmentation tasks. The results demonstrate that our MogaNet establishes new state-of-the-art over other popular methods in mainstream scenarios and all model scales. Typically, the lightweight MogaNet-T achieves 80.0% top-1 accuracy with only 1.44G FLOPs using refined training setup on ImageNet-1K, surpassing ParC-Net-S by 1.4% accuracy but saving 59% (2.04G) FLOPs.

1. Introduction

Convolutional Neural Networks (ConvNets) have been the method of choice for computer vision [42, 58, 93] since the rise of deep neural networks (DNNs) [59]. Inspired by primate visual systems [60, 99, 134], a convolutional layer can encode neighborhood correlations of observed images with regional dense connection and translation-equivariance constraints. By interleaving hierarchical layers, ConvNets attain passively increasing receptive fields [79] and are adept at recognizing underlying semantical patterns. Despite the high performance, representations extracted by ConvNets have been proven to have a strong bias on regional texture [112], resulting in a significant loss of global

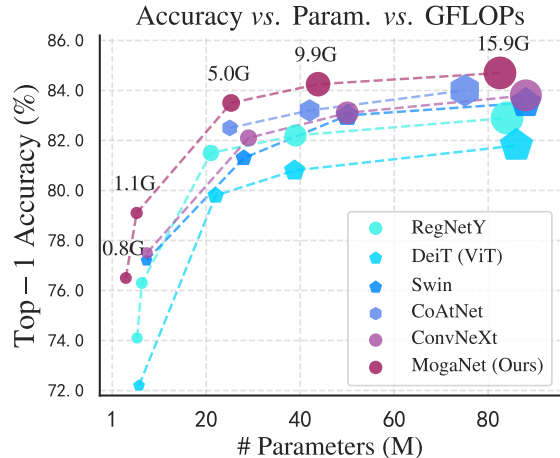


Figure 1. **Performance of models on ImageNet-1K validation set.** Our proposed pure convolution-based MogaNet outperforms previous Transformers (DeiT [106] and Swin [73]), ConvNets (RegNetY [90] and ConvNeXt [74]), and hybrid architectures (CoAtNet [23]) at all parameter scales.

context for visual objects [5, 29, 46, 46]. To address this limitation, previous works propose to craft improved macro-architectures [17, 90, 132, 147] and context aggregation modules [51, 121, 123].

In contrast, by relaxing local inductive bias, the newly emerged Vision Transformer (ViT) [31] and its variants [18, 73, 119] have rapidly surpassed ConvNets on a wide range of vision benchmarks. There is an almost unanimous consensus that the competence of ViTs primarily stems from the self-attention mechanism [4, 113], which facilitates long-range interactions regardless of the topological distance. From a practical standpoint, however, quadratic complexity within pairwise attentions prohibitively restricts the computational efficiency of ViTs [52, 118, 125] and its application potential to fine-grained downstream tasks [56, 75, 151]. Furthermore, the absence of convolutional inductive bias shatters the inherent 2D structure of images, thereby inevitably inducing the detriment of image-specific neighborhood relationships [87]. As such, several subsequent endeavors have been contributed to reintroduce pyramid-like hierarchical layouts [33, 73, 119] and shift-invariant priors [16, 23, 38, 61, 126] to ViTs.

*Equal contribution † Corresponding author

Different from previous research, recent studies have empirically revealed that the expression superiority of ViTs largely hinges on their macro-level architectures rather than the commonly-conjectured token-mixers [91, 105, 139]. More importantly, with advanced training setup and structure modernization, ConvNets can readily deliver comparable or even superior performance than well-tuned ViTs without increasing computational budgets [29, 74, 87, 122]. Nevertheless, there remains a representation bottleneck for existing approaches [26, 46, 85, 124]: naive implementation of self-attention or large kernels hampers the modeling of discriminative contextual information and global interactions, leading to the cognition gap between DNNs and human visual system. As in feature integration theory [110], human brains not only extract local features but simultaneously aggregate these features for global perception, which is more compact and efficient than DNNs [73, 74].

To address this challenge, we investigate the representation capacity of DNNs from the view of feature interaction complexities. In Figure 3b, most modern DNNs are inclined to encode interactions of extremely low or high complexities rather than the most informative intermediate ones [26]. To this end, we preview a macro ConvNet framework with corresponding essential operations and further develop a novel family of ConvNets called **Multi-order gated aggregation Network (MogaNet)** for expediting contextual information with multiple interaction complexities. In MogaNet, we introduce a multi-order feature aggregation module as per human vision. Our design encapsulates both locality perception and context aggregation into a unified spatial aggregation block, where compound multi-order correlations are efficiently congregated and contextualized with gating mechanism in parallel. From the channel aspect, as existing methods are prone to high channel-wise information redundancy [52, 91], we tailor a simple yet effective channel aggregation block, which performs adaptive channel-wise reallocation to the input features and significantly outperforms prevailing counterparts (*e.g.*, SE module [51]) with lower computational cost.

Extensive experiments demonstrate the impressive performance and efficiency of MogaNet at different model scales on ImageNet-1K and multifarious downstream benchmarks. We empirically prove that interaction complexity can serve as a significant indication, like the receptive field, for high quality visual recognition. As a result, with 1.44G FLOPs and 5.2M parameters, MogaNet-T achieves top-1 accuracy of 79.6% and 80.0% using the default and refined training strategies on ImageNet-1K, surpassing the previous state-of-the-art ParC-Net-S [145] by 1.0% with 2.04G fewer FLOPs under the same setup. Moreover, MogaNet-S attains 83.4% top-1 accuracy with 4.97G FLOPs and 25.3M parameters, yielding a promising computational overhead compared with popular small-size

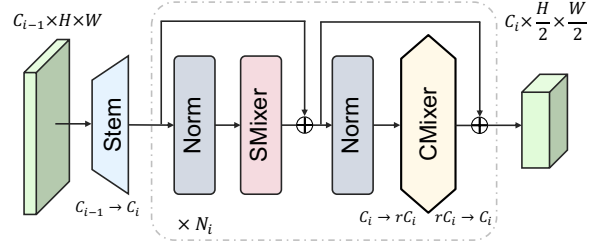


Figure 2. **Illustration of the macro architecture.** It has 4 stages in hierarchical, and each stage i contains an embedding stem and N_i blocks of $\text{SMixer}(\cdot)$ and $\text{CMixer}(\cdot)$ with PreNorm [117] and identical connection [42]. The features within the stage i are kept in the same shape of $C_i \times \frac{H}{2} \times \frac{W}{2}$, except that $\text{CMixer}(\cdot)$ will increase the dimension to rC_i as an inverted bottleneck [94].

models, as shown in Figure 1.

2. Preliminaries

As ViTs greatly surpass canonical ConvNets in many vision tasks, several works try to explain *what* makes ViTs work. We present a comprehensive macro architecture from two aspects, overall framework and essential operations.

2.1. Overall Framework

Recent studies have shown that the inherent framework makes ViTs superior [73, 105, 111]. Therefore, we first introduce a hierarchical design for ConvNets that takes in the merits of ViTs as in Figure 2. It primarily comprises three cardinal components: (i) embedding stem, (ii) spatial mixing block, and (iii) channel mixing block. The embedding stem is a key component in classical ConvNets [42, 132] and ViTs [31, 119], which downsamples the input image to reduce image-inherent redundancies and computational overload. Given X in $H \times W$ resolutions as the input image or the output from the previous stage, we treat the stem as a “size controller” at the start of each stage:

$$Z = \text{Stem}(X), \quad (1)$$

where Z is downsampled to $\frac{H}{2} \times \frac{W}{2}$ resolutions. Then, the feature flows to a stack of residual blocks at each stage. The network modules can be decoupled into two separate components: $\text{SMixer}(\cdot)$ and $\text{CMixer}(\cdot)$ for spatial-wise and channel-wise information propagation [139],

$$Y = X + \text{SMixer}(\text{Norm}(X)), \quad (2)$$

$$Z = Y + \text{CMixer}(\text{Norm}(Y)), \quad (3)$$

where $\text{Norm}(\cdot)$ is a normalization layer, *e.g.*, Batch Normalization [54] (BN). Notice that $\text{SMixer}(\cdot)$ could be various spatial operations (*e.g.*, self-attention [113], convolution), while $\text{CMixer}(\cdot)$ is usually achieved by channel-wise MLP in inverted bottleneck [94] and an expand ratio of r .

2.2. Revisiting Essential Operations

How to learn contextual and robust features effectively is the main theme of visual representation learning. We categorize two types of significant operations that are bound up

with the expression capacities: *regionality perception* and *context aggregation*. Here, we assume the input feature X and the output Z are in the same shape $\mathbb{R}^{C \times H \times W}$.

Regionality Perception Raw images are with local structure and are of high redundant in spatial space. This nature requires operations with local and structural inductive biases to effectively extract contextual representation. We summarize these operations and network modules that *statically* extract contextual features as *regionality perception* and define it as $Z = \mathcal{S}(X, W)$, where $\mathcal{S}(\cdot, \cdot)$ can be an arbitrary binary operator (*e.g.*, dot-product, convolution, element-wise product) and W denotes the learnable weight. Instances of regionality perception are locally connected and weight-sharing on different positions, such as all kinds of convolutions [17, 102, 138], spatial MLP [105], or even non-parametric operations like pooling [139] and spatial shifting [114]. The convolution operation is the most commonly used and thoroughly studied, balancing the efficiency vs. accuracy trade-off [50, 94, 103]. Convolution can be written as $Z = \mathcal{S}(X, K)$, where $\mathcal{S}(\cdot, \cdot)$ is the convolution and the kernel $K \in \mathbb{R}^{M \times C \times k \times k}$ consists M filters.

Context Aggregation Apart from the local features, high-level semantic context modeling is also vital for visual recognition. Classical ConvNets [100, 132] often use deep stacks of these modules to capture the long-range interactions limited by their receptive fields. However, these designs might be computationally inefficient and produce redundant features [43, 50]. To tackle this dilemma, context aggregation modules were proposed to adaptively explore and emphasize the underlying contextual information and decrease trivial redundancies from the input feature. Formally, we summarize *context aggregation* as a family of network components that *adaptively* capture interactions between two embedded features:

$$O = \mathcal{S}(\mathcal{F}_\phi(X), \mathcal{G}_\psi(X)), \quad (4)$$

where $\mathcal{F}_\phi(\cdot)$ and $\mathcal{G}_\psi(\cdot)$ are the aggregation and context branches with parameters ϕ and ψ . Optionally, the output can be transformed to the input dimension by a linear projection, $Z = OW_O$. In contrast to regionality perception, context aggregation modules model the importance of each position on X by the aggregation branch $\mathcal{F}_\phi(X)$ and reweights the embedded feature from the context branch $\mathcal{G}_\psi(X)$ by $\mathcal{S}(\cdot, \cdot)$.

Method	$\mathcal{S}(\cdot, \cdot)$	$\mathcal{F}_\phi(\cdot)$	$\mathcal{G}_\psi(\cdot)$
Self-attention [113]	$\langle \cdot, \cdot \rangle$	$\text{Softmax}(C^{\frac{1}{2}} X W_Q (X W_K)^T)$	$X W_V$
Linear attention [118]	$\langle \cdot, \cdot \rangle$	$\text{Softmax}(C^{\frac{1}{2}} X W_Q (W_E X W_K)^T)$	$W_F X W_V$
GLU [25]	\odot	$\text{Sigmoid}(X W_\phi)$	$X W_\psi$
SE [51]	\odot	$\text{Sigmoid}((\text{GAP}(X) W_\phi) W_\psi)$	X

Table 1. Examples of context aggregation methods according to Eq. (4). The sing-head version of self-attention and linear attention is presented as an illustration and W denotes a linear projection.

We briefly introduce two types of commonly-adopted context aggregations: self-attention mechanism [31, 113, 121] and gating attention [25, 51], as shown in Table 1. Notably, the importance of each position on X is calculated by global interactions of all other positions in $\mathcal{F}_\phi(\cdot)$ with a dot-product. This operation takes quadratic complexity and resulted in large computational overhead. To overcome this limitation, many attention variants in linear complexity [78, 89] were proposed to substitute dot-product self-attention, *e.g.*, linear attention [83, 118] in the second line of Table 1, but they usually introduce inductive biases and might degenerate to trivial attentions [125]. Different from self-attention, gating unit employs an element-wise product \odot as $\mathcal{S}(\cdot, \cdot)$ in linear complexity, *e.g.*, gated linear unit (GLU) variants [96] and squeeze-and-excitation (SE) modules [51] in the last two lines of Table 1. However, they only aggregate the information of each position or the overall context with global average pooling (GAP), which lacks spatial interactions.

3. Representation Bottleneck from the View of Multi-order Interaction

The analysis of DNNs’ representation capability delivers a new perspective to explain and recognize existing DNNs. In contrast to previous studies that mainly center on the robustness and generalization ability of DNNs [82, 85, 150], we expand the scope to the investigation of feature interaction complexities. Intuitively, as shown in Figure 3a, the powerful ViTs can still recognize the target object under extreme occlusion ratios (*e.g.*, only 10~20% visible patches) but produce limited information gain with intermediate oc-

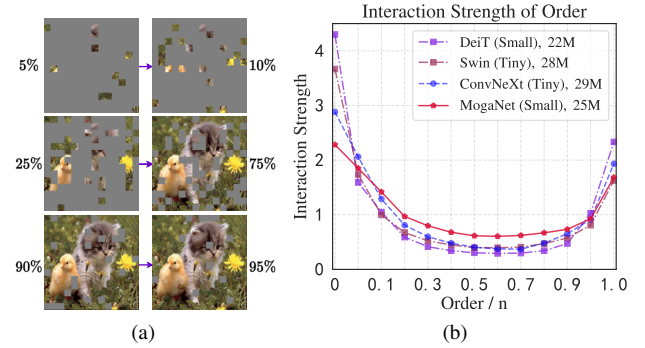


Figure 3. (a) **Illustrations of representation bottleneck.** Humans can recognize the object from images with around 50% patches while learning little new information with a few (*e.g.*, 5~10%) or almost all patches (*e.g.*, 90~95%). DNNs are inclined to extract the most information from very few or the most patches but usually have little information gain with 25~75% patches. (b) **Distributions of the interaction strength** $J^{(m)}$ are plotted for Transformers (DeiT and Swin) and ConvNets (ConvNeXt and MogaNet) on ImageNet-1K with 224^2 resolutions and $n = 14 \times 14$. Middle-order interactions mean the middle-complex interaction, where a medium number of patches (*e.g.*, 0.2~0.8n) participate.

clusions [26], which indicates a cognition gap between prevailing deep models and human vision. It can be explained by m -th order interaction $I^{(m)}(i, j)$ and m -order interaction strength $J^{(m)}$, as defined in [26, 146]. Considering the image with n patches in total, $I^{(m)}(i, j)$ measures the average interaction complexity between the patch pair i, j on all contexts consisting of m patches, where $0 \leq m \leq n-2$ and the order m reflects the contextual complexity. Normalized by the average of interaction strength, the relative interaction strength $J^{(m)}$ with $m \in (0, 1)$ measures the complexity of interactions encoded in DNNs. Refer to Appendix B.1 for definitions and details. Along this line, we show empirically in Figure 3b that most current DNNs are more favored to encode excessively low-order or high-order interactions while typically missing the most informative middle-order ones. From our perspective, such a representation bottleneck might attribute to the inappropriate combination of aforementioned regionality perception and context aggregation operations [26, 64, 110, 112], which infuses unfavorable interaction bias into deep architectures.

4. Methodology

4.1. Overview of MogaNet

Figure A1 provides an illustration of the four-stage MogaNet architecture. For stage i , the input image or feature is first fed into the embedding stem to regulate the feature resolutions and embed into C_i dimensions. Assuming the input image in $H \times W$ resolutions, features of the four stages are in $\frac{H}{4} \times \frac{W}{4}$, $\frac{H}{8} \times \frac{W}{8}$, $\frac{H}{16} \times \frac{W}{16}$, and $\frac{H}{32} \times \frac{W}{32}$ resolution respectively. Then, the embedded feature flows into N_i Moga Blocks, consisting of spatial and channel aggregation blocks as presented in Sec. 4.2 and Sec. 4.3, for further context extraction and aggregation. GAP and a linear layer will be added after the final output for classification tasks. As for dense prediction tasks [41, 93, 130], the output from four stages can be used through neck modules [58, 68].

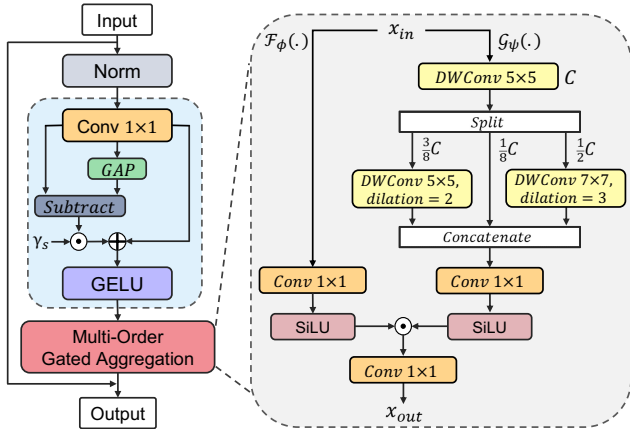


Figure 4. Structure of our proposed spatial aggregation block.

4.2. Multi-order Gated Aggregation

Feature integration theory [110] showed that human vision perceives the object by extracting basic contextual features and associating individual features with attention. However, as we empirically discussed in Sec. 3, the sole presence of regionality perceptions or context aggregation is insufficient to learn diverse contextual features and multi-order interactions simultaneously [26, 61, 87]. Figure 3b shows conventional DNNs tend to focus on low or high-order interactions. They are missing the most informative middle-order interactions. Thus, the primary challenge is how to capture contextual multi-order interactions effectively and efficiently. To this end, we propose a spatial aggregation (SA) block as SMixer(\cdot) to aggregate multi-order contexts in a unified design, as shown in Figure 4, which consists of two cascaded components:

$$Z = X + \text{Moga}\left(\text{FD}(\text{Norm}(X))\right), \quad (5)$$

where $\text{FD}(\cdot)$ is a feature decomposition module (FD) and $\text{Moga}(\cdot)$ is a multi-order gated aggregation module comprising the gating $\mathcal{F}_\phi(\cdot)$ and the context branch $\mathcal{G}_\psi(\cdot)$.

Multi-order contextual features. As a pure convolutional structure, we extract multi-order features with both *static* and *adaptive* regionality perceptions. Except for m -order interactions, there are two trivial interactions, 0-order interaction of each patch itself and 1-order interaction covering all patches, which can be modeled by $\text{Conv}_{1 \times 1}(\cdot)$ and $\text{GAP}(\cdot)$. To force the network focus on the multi-order interactions, we propose $\text{FD}(\cdot)$ to dynamically exclude trivial interactions, which is formulated as:

$$Y = \text{Conv}_{1 \times 1}(X), \quad (6)$$

$$Z = \text{GELU}\left(Y + \gamma_s \odot (Y - \text{GAP}(Y))\right), \quad (7)$$

where $\gamma_s \in \mathbb{R}^{C \times 1}$ is a scaling factor initialized as zeros. By re-weighting the trivial interaction component $Y - \text{GAP}(Y)$, $\text{FD}(\cdot)$ also increase feature diversities [85, 116]. Then, we ensemble depth-wise convolutions (DWConv) to encode multi-order features in the context branch of $\text{Moga}(\cdot)$. Unlike previous works [83, 92, 98, 145] that combine the normal DWConv and self-attentions to model local and global interactions, we employ three DWConv layers with dilation ratios $d \in \{1, 2, 3\}$ in parallel to capture low, middle, and high-order interactions: given the input feature $X \in \mathbb{R}^{C \times HW}$, $\text{DW}_{5 \times 5, d=1}$ is first applied for low-order features; then, the output is factorized into $X_l \in \mathbb{R}^{C_l \times HW}$, $X_m \in \mathbb{R}^{C_m \times HW}$, and $X_h \in \mathbb{R}^{C_h \times HW}$ along the channel dimension, where $C_l + C_m + C_h = C$; afterward, X_l and X_h are assigned to $\text{DW}_{5 \times 5, d=2}$ and $\text{DW}_{7 \times 7, d=3}$, respectively, while X_l serves as identical mapping; finally, the output of X_l , X_m , and X_h are concatenated as multi-order contexts, $Y_C = \text{Concat}(Y_l, Y_m, Y_h)$. Notice that

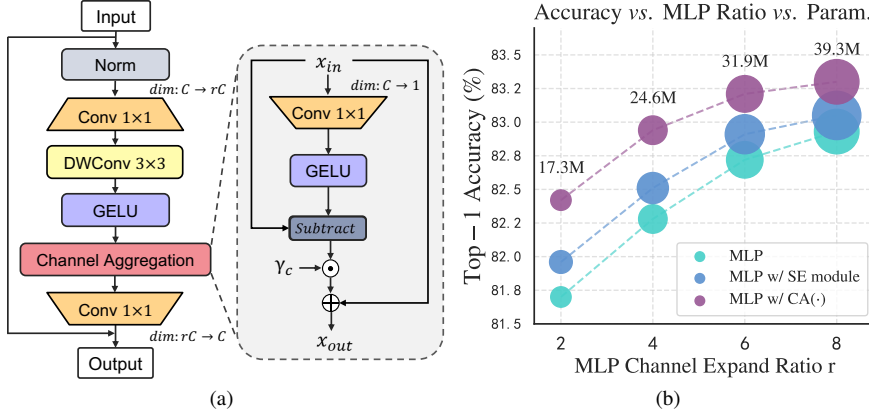


Figure 5. (a) Structure of our proposed channel aggregation block. (b) Analysis of channel MLP and the channel aggregation module. Based on MogaNet-S, performances and model sizes of the raw channel MLP, MLP with SE block, and the channel aggregation is compared with the MLP ratio of $\{2, 4, 6, 8\}$ on ImageNet-1k.

the proposed $FD(\cdot)$ and multi-order $DWConv$ layers only require a little extra computational overhead and parameters than $DW_{7 \times 7}$ used in ConvNeXt [74], *e.g.*, +multi-order and + $FD(\cdot)$ increase 0.04M parameters and 0.01G FLOPs over $DW_{7 \times 7}$ as shown in Table 2.

Gating aggregation. To aggregate the output contexts from the context branch, we employ SiLU [32] activation in the gating branch, *i.e.*, $x \cdot \text{Sigmoid}(x)$, which can be regarded an advanced version of Sigmoid. As verified in Appendix C.1, we find SiLU has both the gating effects as Sigmoid and the stable training property. Taking the output from $FD(\cdot)$ as the input, we rewrite Eq. (4) for Moga(X):

$$Z = \underbrace{\text{SiLU}(\text{Conv}_{1 \times 1}(X))}_{\mathcal{F}_\phi} \odot \underbrace{\text{SiLU}(\text{Conv}_{1 \times 1}(Y_C))}_{\mathcal{G}_\psi}, \quad (8)$$

With the proposed SA blocks, MogaNet captures much more middle-order interactions, as validated in Figure 3b. The SA block produces high-quality multi-order representations with similar parameters and FLOPs as ConvNeXt, which is well beyond the reach of existing methods without applying cost-consuming aggregation (*e.g.*, self-attention).

4.3. Multi-order Features Reallocation by Channel Aggregation

As discussed in Sec. 2.1, mainstream architectures perform channel-mixing CMixer(\cdot) merely by two linear projections, *e.g.*, 2-layer channel MLP [31, 73, 105] with a channel expand ratio r or the MLP with a 3×3 $DWConv$ in between [83, 84, 120]. As plotted in Figure 5b, the vanilla channel MLP requires numerous parameters (r default to 4 or 8) to achieve expected performance, having low computational efficiency. This problem might be caused by redundancy cross channels [10, 103, 115, 123], and most approaches address this issue by improving feature diversity, *e.g.*, inserting a SE module [51] into MLP. Different from

Modules	Top-1 Acc (%)	Params. (M)	FLOPs (G)
Baseline	76.5	4.75	1.01
+Gating branch	77.2	5.09	1.07
+ $DW_{7 \times 7}$	77.4	5.14	1.09
+Multi-order $DW(\cdot)$	77.9	5.17	1.10
+ $FD(\cdot)$	78.2	5.18	1.10
+SE module	78.4	5.29	1.14
+CA(\cdot)	78.9	5.20	1.10

Table 2. Ablation of the designed modules on ImageNet-1K. The baseline adopts the MogaNet framework using the non-linear projection and $DW_{5 \times 5}$ as SMixer(\cdot) and the vanilla MLP as CMixer(\cdot). Gray denotes the final applied modules. In comparison to $DW_{7 \times 7}$ and SE modules, Multi-order $DW(\cdot)$ + $FD(\cdot)$ as multi-order regionality perceptions and CA(\cdot) bring significant improvements with a little extra cost.

previous designs requiring another MLP bottleneck, we design a lightweight channel aggregation module CA(\cdot) to re-weight the high-dimensional hidden spaces and further extend it to a channel aggregation (CA) block. As shown in Figure 5a, the output of our CA block is written as:

$$Y = \text{GELU}\left(DW_{3 \times 3}\left(\text{Conv}_{1 \times 1}(\text{Norm}(X))\right)\right), \quad (9)$$

$$Z = \text{Conv}_{1 \times 1}(CA(Y)) + X.$$

Concretely, CA(\cdot) is implemented by a channel-reduce projection $W_r: \mathbb{R}^{C \times HW} \rightarrow \mathbb{R}^{1 \times HW}$ and GELU to gather and reallocated channel-wise information:

$$CA(X) = X + \gamma_c \odot (X - \text{GELU}(XW_r)), \quad (10)$$

where γ_c is the channel-wise scaling factor. Figure 5b verifies the efficiency of CA(\cdot) in comparison to the vanilla MLP and the MLP with SE module. Despite some improvements to the baseline, the MLP w/ SE module still requires large MLP ratios (*e.g.*, $r = 6$) to achieve expected performance while introducing extra parameters and computational overhead. In contrast, our proposed CA(\cdot) with $r = 4$ brings 0.6% gain over the baseline at a small extra cost (0.04M extra parameters and 0.01G FLOPs) while achieving the same performance as the baseline with $r = 8$.

4.4. Implementation Details

Following the network design style of ConvNets [37, 42, 74], we design MogaNet of five different model sizes (X-Tiny, Tiny, Small, Base, and Large) via stacking the different number of spatial and channel aggregation blocks at each stage, which has similar numbers of parameters as RegNet [90] variants (400MF, 800MF, 4GF, 8GF, and 16GF). Detailed configurations and hyper-parameters are shown in Table A1. We set the channels of the multi-order $DWConv$ layers to $C_l: C_m: C_h = 1:3:4$ (discussed in Appendix C.2). Similar to [61, 66, 108], the first embedding

stem in MogaNet is designed as two stacked 3×3 convolution layers with the stride of 2 while adopting the single-layer version for embedding stems in other three stages. We select GELU [44] as the common activation function and only use SiLU in the Moga module as Eq. (8).

5. Experiments

To verify the effectiveness of our method, we conduct extensive experiments on ImageNet-1K (IN-1K) [27] for image classification, COCO [69] for object detection and instance segmentation, and ADE20K [149] for semantic segmentation. All experiments are implemented with PyTorch on Ubuntu workstations with NVIDIA A100 GPUs. **Bold** and **gray** indicate the best performance and our models.

5.1. ImageNet Classification

Settings. For classification experiments on ImageNet-1K, we train MogaNet variants following the standard procedure [73, 106] for a fair comparison. Specifically, the models are trained for 300 epochs by AdamW [77] optimizer with 224^2 or 256^2 resolutions, a basic learning rate $lr = 1 \times 10^{-3}$, 5 epochs warmup, and a Cosine scheduler [76]. See Appendix A.2 for implementation details. We compare four typical architectures: (i) **Classical ConvNets** include ResNet, SENet, ShuffleNetV2, EfficientNet, MobileNetV3, and RegNet. (ii) **Transformers** include DeiT, Swin, T2T-ViT, PVT, Focal, ViT-C, CSWin, SReT, and LiTV2. (iii) **Hybrid architectures** of attention and convolution include PiT, LeViT, CoaT, BoTNet, ViTAE, Twins, CoAtNet, MobileViT, Uniformer, MobileFormer, ParC-Net, EfficientFormer, and MaxViT. (iv) **Modern ConvNets** include ConvNeXt, RepLkNet, FocalNet, VAN, SLak, and HorNet.

Results. We compare the image classification performances of four widely adopted model sizes (around 5M, 25M, 45M, and 80M parameters). As for lightweight models, Table 3 shows that MogaNet-XT/T significantly outperforms existing lightweight architectures. Using the default training settings, MogaNet-T achieves 79.0% top-1 accuracy, which improves models with around 5M parameters by at least 1.1% using 224^2 resolutions, while outperforming the current best backbone ParC-Net-S by 1.0% using 256^2 resolutions. Meanwhile, MogaNet-XT also surpasses models with 3M parameters, *e.g.*, +4.6% and +1.5% over T2T-ViT-7 and MobileViT-XS. Particularly, MogaNet-T[§] achieves 80.0% top-1 accuracy using 256^2 resolutions and the refined settings, which adjusts lr and replaces RandAugment [21] with 3-Augment [109] as detailed in Appendix C.4. As for small-size models, Table 4 shows MogaNet-S achieves 83.4% top-1 accuracy, which consistently outperforms Transformers, hybrid architectures, and ConvNets, *e.g.*, +2.1% and +1.2% over Swin-T and

Architecture	Date	Image Size	Param. (M)	FLOPs (G)	Top-1 Acc (%)
ResNet-18 [†] [42]	CVPR'2016	224^2	11.7	1.80	71.5
ShuffleNetV2 $2 \times$ [80]	ECCV'2018	224^2	5.5	0.60	75.4
EfficientNet-B0 [103]	ICML'2019	224^2	5.3	0.39	77.1
MobileNetV3 $1 \times$ [49]	ICCV'2019	224^2	5.4	0.23	75.2
RegNetY-400MF [90]	CVPR'2020	224^2	5.3	0.40	74.1
RegNetY-800MF [90]	CVPR'2020	224^2	6.3	0.80	76.3
DeiT-T [106]	ICML'2021	224^2	5.7	1.08	72.2
PVT-T [119]	ICCV'2021	224^2	13.2	1.60	75.1
T2T-ViT-12 [141]	ICCV'2021	224^2	6.9	1.80	76.5
ViT-C [131]	NIPS'2021	224^2	4.6	1.10	75.3
SReT-T _{Distill} [97]	ECCV'2022	224^2	4.8	1.10	77.6
PiT-Ti [45]	ICCV'2021	224^2	4.9	0.70	74.6
LeViT-S [34]	ICCV'2021	224^2	7.8	0.31	76.6
CoaT-Lite-T [65]	ICCV'2021	224^2	5.7	1.60	77.5
Swin-1G [73]	ICCV'2021	224^2	7.3	1.00	77.3
MobileViT-XS [81]	ICLR'2022	256^2	2.3	1.73	74.8
MobileViT-S [81]	ICLR'2022	256^2	5.6	4.02	78.4
MobileFormer-294M [16]	CVPR'2022	224^2	11.4	0.59	77.9
ConvNeXt-XT [74]	CVPR'2022	224^2	7.4	0.60	77.5
VAN-B0 [37]	arXiv'2022	224^2	4.1	0.88	75.4
ParC-Net-S [145]	ECCV'2022	256^2	5.0	3.48	78.6
MogaNet-XT	Ours	224^2	3.0	0.80	76.5
MogaNet-T	Ours	224^2	5.2	1.10	79.0
MogaNet-T	Ours	256^2	5.2	1.44	79.6
MogaNet-T[§]	Ours	256^2	5.2	1.44	80.0

Table 3. **ImageNet-1K classification** performance of lightweight (around 5M parameters) models. [†] and [§] denote using RSB A2 [122] setting for ConvNets and the refined setting for MogaNet.

Architecture	Date	Image Size	Param. (M)	FLOPs (G)	Top-1 Acc (%)
ResNet-50 [†] [42]	CVPR'2016	224^2	26	4.1	80.4
EfficientNet-B4 [103]	ICML'2019	380^2	19	4.2	82.9
RegNetY-4GF [†] [90]	CVPR'2020	224^2	21	4.0	81.5
DeiT-S [106]	ICML'2021	224^2	22	4.6	79.8
Swin-T [73]	ICCV'2021	224^2	28	4.5	81.3
T2T-ViT-14 [141]	ICCV'2021	224^2	22	6.1	81.7
CSWin-T [30]	CVPR'2022	224^2	23	4.3	82.8
SReT-S [97]	ECCV'2022	224^2	21	4.2	81.9
LITV2-S [83]	NIPS'2022	224^2	28	3.7	82.0
CoaT-S [65]	ICCV'2021	224^2	22	12.6	82.1
CoAtNet-0 [23]	NIPS'2021	224^2	25	4.2	82.7
ViTAE-S [133]	NIPS'2021	224^2	24	5.6	82.0
UniFormer-S [61]	ICLR'2022	224^2	22	3.6	82.9
EfficientFormer-L3 [66]	NIPS'2022	224^2	31	3.9	82.4
ConvNeXt-T [74]	CVPR'2022	224^2	29	4.5	82.1
VAN-B2 [37]	arXiv'2022	224^2	27	5.0	82.8
SLaK-T [70]	arXiv'2022	224^2	30	5.0	82.5
HorNet-T _{7×7} [92]	NIPS'2022	224^2	22	4.0	82.8
MogaNet-S	Ours	224^2	25	5.0	83.4

Table 4. **ImageNet-1K classification** performance of small size (around 25M parameters) models.

ConvNeXt-T. As for 45M and 80M models, we summarize their performances in Table 5 and Table 6 and MogaNet-B/L still surpass the current state-of-the-art architectures, especially improving Swin-S/B and ConvNeXt-S/B by 1.2%/1.1% and 1.1%/0.8%. MogaNet also outperforms recently proposed modern ConvNets, *e.g.*, +0.9% over RepLkNet-31B and +0.2%/0.3% over HorNet-S/B_{7×7}.

Architecture	Date	Image Size	Param. (M)	FLOPs (G)	Top-1 Acc (%)
ResNet-101 [†] [42]	CVPR'2016	224 ²	45	7.9	81.5
EfficientNet-B6 [103]	ICML'2019	528 ²	43	19.0	84.0
RegNetY-8GF [†] [90]	CVPR'2020	224 ²	39	8.1	82.2
T2T-ViT-24 [141]	ICCV'2021	224 ²	64	13.2	82.2
Swin-S [73]	ICCV'2021	224 ²	50	8.7	83.0
Focal-S [136]	NIPS'2021	224 ²	51	9.1	83.6
CSWin-S [30]	CVPR'2022	224 ²	35	6.9	83.6
LITV2-M [83]	NIPS'2022	224 ²	49	7.5	83.3
Coat-M [65]	ICCV'2021	224 ²	45	9.8	83.6
Twins-SVT-B [18]	NIPS'2021	224 ²	56	8.6	83.2
CoAtNet-1 [23]	NIPS'2021	224 ²	42	8.4	83.3
UniFormer-B [61]	ICLR'2022	224 ²	50	8.3	83.9
FAN-B-Hybrid [150]	ICML'2022	224 ²	50	11.3	83.9
ConvNeXt-S [74]	CVPR'2022	224 ²	50	8.7	83.1
FocalNet-S (LRF) [135]	NIPS'2022	224 ²	50	8.7	83.5
HorNet-S _{7×7} [92]	NIPS'2022	224 ²	50	8.8	84.0
VAN-B3 [37]	arXiv'2022	224 ²	45	9.0	83.9
SLaK-S [70]	arXiv'2022	224 ²	55	9.8	83.8
MogaNet-B	Ours	224 ²	44	9.9	84.2

Table 5. **ImageNet-1K classification** performance of medium size (around 45M parameters) models.

5.2. Dense Prediction Tasks

Object detection and segmentation on COCO. We evaluate MogaNet for object detection and segmentation tasks on the COCO dataset using Mask-RCNN [41] as the detector. Following the training and evaluation settings in [73], we fine-tune the models with AdamW optimizer for $1\times$ training schedule (12-epoch) on the COCO *train2017* and evaluate on the COCO *val2017*. We adopt MMDetection [14] as the codebase and measure the performance by the box mAP (AP^{bb}) and mask mAP (AP^{mk}). Refer to Appendix A.3 for more details. Table 7 shows that models with MogaNet-T/S/B significantly outperform all previous backbones. Specifically, MogaNet-T gains 3.6% AP^{bb} and 4.6% AP^{mk} over ResNet-18; MogaNet-S outperforms Swin-T (Transformers) by 3.9% AP^{bb} and 2.7% AP^{mk} , and surpasses UniFormer-S (hybrid) by 0.5% AP^{bb} ; MogaNet-B outperforms Swin-T and LITV2-M (Transformer) by 2.9% AP^{bb} and 1.2% AP^{mk} respectively.

Semantic segmentation on ADE20K. We then evaluate MogaNet for semantic segmentation tasks on the ADE20K dataset using Semantic FPN [58] and UperNet [130] following the evaluation schemes in [73, 139]. All experiments are implemented on MMSegmentation [19] codebase, and the performance is measured by mIoU (single scale). Based on Semantic FPN, the models are fine-tuned for 80K iterations by the AdamW optimizer. In Table 8, MogaNet-S consistently outperforms previous architectures, *e.g.*, +6.6% over Swin-T (Transformer), +1.5% over UniFormer-S (hybrid). Based on UperNet, the models are fine-tuned 160K by AdamW optimizer. In Table 8, the models with MogaNet-S improves backbones of Transformers (+3.1% over Swin-T), hybrid architectures (+1.6% over UniFormer-S), and mod-

Architecture	Date	Image Size	Param. (M)	FLOPs (G)	Top-1 Acc (%)
ResNet-152 [†] [42]	CVPR'2016	224 ²	60	11.6	82.0
SE-ResNet-154 [†] [51]	CVPR'2018	224 ²	115	20.9	81.7
RegNetY-16GF [90]	CVPR'2020	224 ²	84	16.0	82.9
DeiT-B [106]	ICML'2021	224 ²	86	17.5	81.8
Swin-B [73]	ICCV'2021	224 ²	89	15.4	83.5
Focal-B [136]	NIPS'2021	224 ²	90	16.4	84.0
CSWin-B [30]	CVPR'2022	224 ²	78	15.0	84.2
LITV2-B [83]	NIPS'2022	224 ²	87	13.2	83.6
BoTNet-T7 [101]	CVPR'2021	256 ²	79	19.3	84.2
Twins-SVT-L [18]	NIPS'2021	224 ²	99	15.1	83.7
CoAtNet-2 [23]	NIPS'2021	224 ²	75	15.7	84.1
FAN-B-Hybrid [150]	ICML'2022	224 ²	77	16.9	84.3
ConvNeXt-B [74]	CVPR'2022	224 ²	89	15.4	83.8
RepLkNet-31B [29]	CVPR'2022	224 ²	79	15.3	83.5
FocalNet-B (LRF) [135]	NIPS'2022	224 ²	89	15.4	83.9
HorNet-B _{7×7} [92]	NIPS'2022	224 ²	87	15.6	84.3
VAN-B4 [37]	arXiv'2022	224 ²	60	12.2	84.2
SLaK-B [70]	arXiv'2022	224 ²	95	17.1	84.0
MogaNet-L	Ours	224 ²	83	15.9	84.6

Table 6. **ImageNet-1K classification** performance of large size (around 80M parameters) models.

ern ConvNets (+1.1% over HorNet-T_{7×7}). Refer to Appendix A.4 for more details.

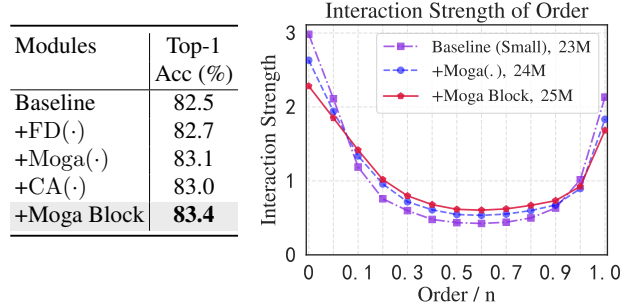


Figure 6. **Ablation of the proposed modules on ImageNet-1K.** **Left:** the table verifies each proposed module based on the baseline of MogaNet-S. **Right:** the figure plots distributions of the interaction strength $J^{(m)}$ and verifies that Moga(·) contributes the most to learning multi-order interactions and better performance.

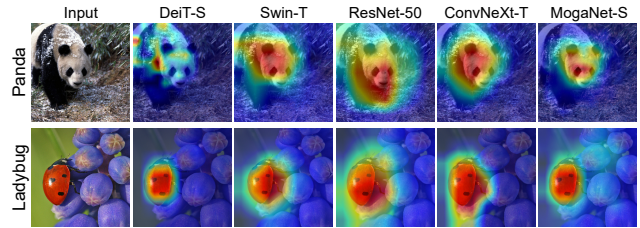


Figure 7. **Grad-CAM activation maps of models trained on ImageNet-1K.** MogaNet-S shows similar activation maps as local attention architectures (Swin-T), which are located on the semantic targets. Unlike the results of previous ConvNets, which might activate some irrelevant parts, the activation maps of MogaNet-S are more gathered. See more visualizations in Appendix B.2.

5.3. Ablation and Analysis

We first ablate the spatial aggregation module, including FD(·) and Moga(·), which contains the **gating branch**

Method	Date	Param. FLOPs		Mask R-CNN 1×						
		(M)	(G)	AP ^{bb}	AP ^{bb} ₅₀	AP ^{bb} ₇₅	AP ^{mk}	AP ^{mk} ₅₀	AP ^{mk} ₇₅	
ResNet-18 [42]	CVPR'2016	31	207	34.0	54.0	36.7	31.2	51.0	32.7	
PVT-T [119]	ICCV'2021	33	208	36.7	59.2	39.3	35.1	56.7	37.3	
MogaNet-T	Ours	28	195	37.6	60.5	40.2	35.8	57.6	37.8	
ResNet-50 [42]	CVPR'2016	44	260	38.0	58.6	41.4	34.4	55.1	36.7	
PVT-S [119]	ICCV'2021	44	245	40.4	62.9	43.8	37.8	60.1	40.3	
Swin-T [73]	ICCV'2021	48	264	42.2	64.6	46.2	39.1	61.6	42.0	
FocalNet-T [136]	NIPS'2021	49	291	44.8	67.7	49.2	41.0	64.7	44.2	
Uniformer-S [61]	ICLR'2022	41	269	45.6	68.1	49.7	41.6	64.8	45.0	
LITV2-S [83]	NIPS'2022	47	261	44.9	67.0	49.5	40.8	63.8	44.2	
MogaNet-S	Ours	45	260	46.1	68.3	50.1	41.8	65.1	44.9	
ResNet-101 [42]	CVPR'2016	63	336	40.4	61.1	44.2	36.4	57.7	38.8	
PVT-M [119]	ICCV'2021	64	302	42.0	64.4	45.6	39.0	61.6	42.1	
Swin-T [73]	ICCV'2021	69	354	44.8	66.6	48.9	40.9	63.4	44.2	
FocalNet-S [136]	NIPS'2021	71	401	47.4	69.8	51.9	42.8	66.6	46.1	
UniFormer-B [61]	ICLR'2022	69	399	47.4	69.7	52.1	43.1	66.0	46.5	
LITV2-M [83]	NIPS'2022	68	315	46.5	68.0	50.9	42.0	65.1	45.0	
MogaNet-B	Ours	68	342	47.9	70.0	52.7	43.2	67.0	46.6	

Table 7. **Object detection and instance segmentation** with Mask R-CNN (1× training schedule) on COCO *val2017*. The FLOPs are measured at res- resolution 800 × 1280.

and the context branch with **multi-order DWConv layers**, and the **channel aggregation** module CA(·). As verified in Table 2 and Figure 6 (left), all proposed modules yield improvements with a few costs. Appendix C provides more ablation studies. Furthermore, we empirically verify the multi-order interactions in Figure C.2 (right) and visualize class activation maps (CAM) by Grad-CAM [95] in comparison to existing models in Figure 7.

6. Related Work

Convolutional Neural Networks ConvNets [42, 59, 60] have dominated a wide scope of computer vision (CV) tasks for decades. ResNet [42] introduces an identity skip connection and a bottleneck module that alleviates training difficulties (*e.g.*, vanishing gradient). ResNet and its variants [51, 132, 143, 147] have become the most widely-adopted ConvNet architectures in numerous CV applications. For practical usage, many efficient models [49, 50, 80, 90, 94, 103] are designed for a complexity-accuracy trade-off and hardware devices. Since the limited reception field of spatial and temporal convolutions struggles to capture global dependency [79], various spatial-wise or channel-wise attention strategies [10, 22, 51, 121, 123] are designed. Recently, taking merits of the macro design of Transformers [31], modern ConvNets [29, 70, 74, 92, 111, 135] show thrilling performance with large depth-wise convolutions [39] for local context and long-range aggregation.

Vision Transformers Transformer [113] with the self-attention mechanism has become the mainstream choice in the natural language processing (NLP) community [9, 28]. Considering that global information is also essential for CV tasks, Vision Transformer (ViT) [31] is proposed and has achieved promising results on ImageNet [27]. In particular, ViT splits raw images into non-overlapping fixed-size

	Method	Date	Param. FLOPs		mIoU ^{ss}
			(M)	(G)	(%)
Semantic FPN (80K)	ResNet50 [42]	CVPR'2016	29	183	36.7
	PVT-S [119]	ICCV'2021	28	161	39.8
	Twins-S [18]	NIPS'2021	28	162	44.3
	Swin-T [73]	ICCV'2021	32	182	41.5
	Uniformer-S [61]	ICLR'2022	25	247	46.6
	LITV2-S [83]	NIPS'2022	31	179	44.3
	VAN-B2 [37]	arXiv'2022	30	164	46.7
	MogaNet-S	Ours	29	180	48.1
UperNet (160K)	ResNet-101 [42]	CVPR'2016	86	1029	44.9
	DeiT-S [106]	ICML'2021	52	1099	44.0
	Swin-T [73]	ICCV'2021	60	945	46.1
	ConvNeXt-T [74]	CVPR'2022	60	939	46.7
	Twins-S [18]	NIPS'2021	54	901	46.2
	UniFormer-S [61]	ICLR'2022	52	1008	47.6
	HorNet-T _{7×7} [92]	NIPS'2022	52	926	48.1
	MogaNet-S	Ours	56	932	49.2

Table 8. **Semantic segmentation** with semantic FPN (80K schedule) and UperNet (160K schedule) on ADE20K. The FLOPs are measured at resolution 512 × 2048.

patches as visual tokens to capture long-range feature interactions among these tokens by self-attention. By introducing regional inductive bias, ViT and its variants have been extended to various vision tasks [2, 11, 13, 56, 86, 151]. Equipped with advanced training strategies [106, 107, 109, 140] or extra knowledge [57, 67, 128], pure ViTs can achieve competitive performance as ConvNets in CV tasks. In the literature of [139], the MetaFormer architecture substantially influenced the design of vision backbones, and all Transformer-like models [106, 111, 114] are classified by how they treat the token-mixing approaches, such as relative position encoding [127], local window shifting [73] and MLP layer [105], *etc.* Compared to ConvNets banking on the inherent inductive biases (*e.g.*, locality and translation equivariance), the pure ViTs are more over-parameterized and rely on large-scale pre-training [6, 31, 40, 64] to a great extent. Targeting this problem, one branch of researchers proposes lightweight ViTs [15, 66, 81, 131] with more efficient self-attentions variants [118]. Meanwhile, the incorporation of self-attention and convolution as a hybrid backbone has been vigorously studied [23, 24, 36, 61, 84, 98, 126] for imparting regional priors to ViTs.

7. Conclusion

In this work, we present a novel pure ConvNet for visual representation learning named MogaNet. Specifically, we design a spatial aggregation block and an adaptive channel aggregation block to capture contextual representations and multi-order interactions under the complexity-performance trade-off paradigm. Extensive experiments verify the substantial superiority of MogaNet, compared to state-of-the-art ConvNets, ViTs, and hybrid architectures across mainstream vision tasks. Overall, we hope MogaNet can be more than a commodity but also inspire the way toward the further quest of architecture design for computer visual tasks.

Acknowledgement

This work was done during the internship of Zedong Wang and Zhiyuan Chen at Westlake University. We thank the AI Station of Westlake University for the support of GPUs. We thank Mengzhao Chen for polishing the writing of the manuscript.

References

- [1] Marco Ancona, Cengiz Oztireli, and Markus Gross. Explaining deep neural networks with a polynomial time algorithm for shapley value approximation. In *International Conference on Machine Learning (ICML)*, pages 272–281. PMLR, 2019. 16
- [2] Anurag Arnab, Mostafa Dehghani, Georg Heigold, Chen Sun, Mario Lučić, and Cordelia Schmid. Vivit: A video vision transformer. In *IEEE International Conference on Computer Vision (ICCV)*, 2021. 8
- [3] Jimmy Ba, Jamie Ryan Kiros, and Geoffrey E. Hinton. Layer normalization. *ArXiv*, abs/1607.06450, 2016. 17
- [4] Dzmitry Bahdanau, Kyunghyun Cho, and Yoshua Bengio. Neural machine translation by jointly learning to align and translate. In *International Conference on Learning Representations (ICLR)*, 2015. 1
- [5] Nicholas Baker, Hongjing Lu, Gennady Erlikhman, and Philip J. Kellman. Deep convolutional networks do not classify based on global object shape. *PLoS Computational Biology*, 14(12):e1006613, 2018. 1
- [6] Hangbo Bao, Li Dong, and Furu Wei. Beit: Bert pre-training of image transformers. In *International Conference on Learning Representations (ICLR)*, 2022. 8, 18
- [7] Andrew Brock, Soham De, and Samuel L. Smith. Characterizing signal propagation to close the performance gap in unnormalized resnets. In *International Conference on Learning Representations (ICLR)*, 2021. 17
- [8] Andrew Brock, Soham De, Samuel L. Smith, and Karen Simonyan. High-performance large-scale image recognition without normalization. *ArXiv*, abs/2102.06171, 2021. 17
- [9] Tom B Brown, Benjamin Mann, Nick Ryder, Melanie Subbiah, Jared Kaplan, Prafulla Dhariwal, Arvind Neelakantan, Pranav Shyam, Girish Sastry, Amanda Askell, et al. Language models are few-shot learners. *Advances in Neural Information Processing Systems (NeurIPS)*, 2020. 8
- [10] Yue Cao, Jiarui Xu, Stephen Lin, Fangyun Wei, and Han Hu. Gnet: Non-local networks meet squeeze-excitation networks and beyond. In *2019 IEEE/CVF International Conference on Computer Vision Workshop (ICCVW)*, pages 1971–1980, 2019. 5, 8
- [11] Nicolas Carion, Francisco Massa, Gabriel Synnaeve, Nicolas Usunier, Alexander Kirillov, and Sergey Zagoruyko. End-to-end object detection with transformers. In *Proceedings of the European Conference on Computer Vision (ECCV)*, 2020. 8
- [12] Mathilde Caron, Hugo Touvron, Ishan Misra, Hervé Jégou, Julien Mairal, Piotr Bojanowski, and Armand Joulin. Emerging properties in self-supervised vision transformers. In *Proceedings of the International Conference on Computer Vision (ICCV)*, 2021. 18
- [13] Hanting Chen, Yunhe Wang, Tianyu Guo, Chang Xu, Yiping Deng, Zhenhua Liu, Siwei Ma, Chunjing Xu, Chao Xu, and Wen Gao. Pre-trained image processing transformer. In *Proceedings of the IEEE/CVF Conference on Computer Vision and Pattern Recognition (CVPR)*, 2021. 8
- [14] Kai Chen, Jiaqi Wang, Jiangmiao Pang, Yuhang Cao, Yu Xiong, Xiaoxiao Li, Shuyang Sun, Wansen Feng, Ziwei Liu, Jiarui Xu, Zheng Zhang, Dazhi Cheng, Chenchen Zhu, Tianheng Cheng, Qijie Zhao, Buyu Li, Xin Lu, Rui Zhu, Yue Wu, Jifeng Dai, Jingdong Wang, Jianping Shi, Wanli Ouyang, Chen Change Loy, and Dahua Lin. MMDetection: Open mmlab detection toolbox and benchmark. <https://github.com/open-mmlab/mmdetection>, 2019. 7, 16
- [15] Mengzhao Chen, Mingbao Lin, Ke Li, Yunhang Shen, Yongjian Wu, Fei Chao, and Rongrong Ji. Cf-vit: A general coarse-to-fine method for vision transformer. *ArXiv*, abs/2203.03821, 2022. 8
- [16] Yinpeng Chen, Xiyang Dai, Dongdong Chen, Mengchen Liu, Xiaoyi Dong, Lu Yuan, and Zicheng Liu. Mobileformer: Bridging mobilenet and transformer. In *Proceedings of the IEEE/CVF Conference on Computer Vision and Pattern Recognition (CVPR)*, 2022. 1, 6, 15
- [17] François Chollet. Xception: Deep learning with depthwise separable convolutions. In *Proceedings of the IEEE conference on computer vision and pattern recognition (CVPR)*, pages 1251–1258, 2017. 1, 3
- [18] Xiangxiang Chu, Zhi Tian, Yuqing Wang, Bo Zhang, Haibing Ren, Xiaolin Wei, Huaxia Xia, and Chunhua Shen. Twins: Revisiting the design of spatial attention in vision transformers. In *Advances in Neural Information Processing Systems (NeurIPS)*, 2021. 1, 7, 8, 17
- [19] MMSegmentation Contributors. MMSegmentation: Open-mmlab semantic segmentation toolbox and benchmark. <https://github.com/open-mmlab/mms Segmentation>, 2020. 7, 16
- [20] Ekin Dogus Cubuk, Barret Zoph, Dandelion Mané, Vijay Vasudevan, and Quoc V. Le. Autoaugment: Learning augmentation strategies from data. *2019 IEEE/CVF Conference on Computer Vision and Pattern Recognition (CVPR)*, pages 113–123, 2019. 15
- [21] Ekin D Cubuk, Barret Zoph, Jonathon Shlens, and Quoc V Le. Randaugment: Practical automated data augmentation with a reduced search space. In *Proceedings of the IEEE/CVF Conference on Computer Vision and Pattern Recognition Workshops (CVPRW)*, pages 702–703, 2020. 6, 15
- [22] Jifeng Dai, Haozhi Qi, Yuwen Xiong, Yi Li, Guodong Zhang, Han Hu, and Yichen Wei. Deformable convolutional networks. In *IEEE International Conference on Computer Vision (ICCV)*, pages 764–773, 2017. 8
- [23] Zihang Dai, Hanxiao Liu, Quoc V Le, and Mingxing Tan. Coatnet: Marrying convolution and attention for all data sizes. *Advances in Neural Information Processing Systems (NeurIPS)*, 34:3965–3977, 2021. 1, 6, 7, 8

- [24] Stéphane d’Ascoli, Hugo Touvron, Matthew Leavitt, Ari Morcos, Giulio Biroli, and Levent Sagun. Convit: Improving vision transformers with soft convolutional inductive biases. *arXiv preprint arXiv:2103.10697*, 2021. 8
- [25] Yann N Dauphin, Angela Fan, Michael Auli, and David Grangier. Language modeling with gated convolutional networks. In *International conference on machine learning (ICML)*, pages 933–941. PMLR, 2017. 3
- [26] Huiqi Deng, Qihan Ren, Xu Chen, Hao Zhang, Jie Ren, and Quanshi Zhang. Discovering and explaining the representation bottleneck of dnns. In *International Conference on Learning Representations (ICLR)*, 2022. 2, 4, 16, 17
- [27] Jia Deng, Wei Dong, Richard Socher, Li-Jia Li, Kai Li, and Li Fei-Fei. ImageNet: A large-scale hierarchical image database. In *Proceedings of the IEEE/CVF Conference on Computer Vision and Pattern Recognition (CVPR)*, 2009. 6, 8, 15
- [28] Jacob Devlin, Ming-Wei Chang, Kenton Lee, and Kristina Toutanova. Bert: Pre-training of deep bidirectional transformers for language understanding. *arXiv:1810.04805*, 2018. 8, 15
- [29] Xiaohan Ding, X. Zhang, Yi Zhou, Jungong Han, Guiguang Ding, and Jian Sun. Scaling up your kernels to 31x31: Revisiting large kernel design in cnns. In *Proceedings of the IEEE/CVF Conference on Computer Vision and Pattern Recognition (CVPR)*, 2022. 1, 2, 7, 8
- [30] Xiaoyi Dong, Jianmin Bao, Dongdong Chen, Weiming Zhang, Nenghai Yu, Lu Yuan, Dong Chen, and Baining Guo. Cswin transformer: A general vision transformer backbone with cross-shaped windows. In *Proceedings of the IEEE/CVF Conference on Computer Vision and Pattern Recognition (CVPR)*, 2022. 6, 7
- [31] Alexey Dosovitskiy, Lucas Beyer, Alexander Kolesnikov, Dirk Weissenborn, Xiaohua Zhai, Thomas Unterthiner, Mostafa Dehghani, Matthias Minderer, Georg Heigold, Sylvain Gelly, et al. An image is worth 16x16 words: Transformers for image recognition at scale. In *International Conference on Learning Representations (ICLR)*, 2020. 1, 2, 3, 5, 8, 17
- [32] Stefan Elfving, Eiji Uchibe, and Kenji Doya. Sigmoid-weighted linear units for neural network function approximation in reinforcement learning. *Neural Networks*, 107:3–11, 2018. 5, 17
- [33] Haoqi Fan, Bo Xiong, Karttikeya Mangalam, Yanghao Li, Zhicheng Yan, Jitendra Malik, and Christoph Feichtenhofer. Multiscale vision transformers. In *Proceedings of the IEEE/CVF International Conference on Computer Vision (ICCV)*, pages 6824–6835, 2021. 1
- [34] Benjamin Graham, Alaaeldin El-Nouby, Hugo Touvron, Pierre Stock, Armand Joulin, Hervé Jégou, and Matthijs Douze. Levit: a vision transformer in convnet’s clothing for faster inference. In *Proceedings of the IEEE/CVF international conference on computer vision (ICCV)*, pages 12259–12269, 2021. 6
- [35] Jean-Bastien Grill, Florian Strub, Florent Altché, Corentin Tallec, Pierre H Richemond, Elena Buchatskaya, Carl Doersch, Bernardo Avila Pires, Zhaohan Daniel Guo, Mohammad Gheshlaghi Azar, et al. Bootstrap your own latent: A new approach to self-supervised learning. In *Advances in Neural Information Processing Systems (NeurIPS)*, 2020. 18
- [36] Jianyuan Guo, Kai Han, Han Wu, Chang Xu, Yehui Tang, Chunjing Xu, and Yunhe Wang. Cmt: Convolutional neural networks meet vision transformers. *arXiv preprint arXiv:2107.06263*, 2021. 8
- [37] Meng-Hao Guo, Cheng-Ze Lu, Zheng-Ning Liu, Ming-Ming Cheng, and Shi-Min Hu. Visual attention network. *arXiv preprint arXiv:2202.09741*, 2022. 5, 6, 7, 8, 15, 17, 19
- [38] Kai Han, An Xiao, Enhua Wu, Jianyuan Guo, Chunjing Xu, and Yunhe Wang. Transformer in transformer. *Advances in Neural Information Processing Systems (NeurIPS)*, 34:15908–15919, 2021. 1
- [39] Qi Han, ZeJia Fan, Qi Dai, Lei Sun, Ming-Ming Cheng, Jiaying Liu, and Jingdong Wang. Demystifying local vision transformer: Sparse connectivity, weight sharing, and dynamic weight. *arXiv:2106.04263*, 2021. 8
- [40] Kaiming He, Xinlei Chen, Saining Xie, Yanghao Li, Piotr Dollár, and Ross Girshick. Masked autoencoders are scalable vision learners. In *Proceedings of the IEEE/CVF Conference on Computer Vision and Pattern Recognition (CVPR)*, 2022. 8
- [41] Kaiming He, Georgia Gkioxari, Piotr Dollár, and Ross Girshick. Mask r-cnn. In *Proceedings of the IEEE/CVF International Conference on Computer Vision (ICCV)*, 2017. 4, 7, 16
- [42] Kaiming He, Xiangyu Zhang, Shaoqing Ren, and Jian Sun. Deep residual learning for image recognition. In *Proceedings of the IEEE conference on computer vision and pattern recognition (CVPR)*, pages 770–778, 2016. 1, 2, 5, 6, 7, 8, 15, 16, 17, 19
- [43] Yihui He, Xiangyu Zhang, and Jian Sun. Channel pruning for accelerating very deep neural networks. In *2017 IEEE International Conference on Computer Vision (ICCV)*, pages 1398–1406, 2017. 3
- [44] Dan Hendrycks and Kevin Gimpel. Bridging nonlinearities and stochastic regularizers with gaussian error linear units. *arXiv preprint arXiv:1606.08415*, 2016. 6, 17
- [45] Byeongho Heo, Sangdoo Yun, Dongyoon Han, Sanghyuk Chun, Junsuk Choe, and Seong Joon Oh. Rethinking spatial dimensions of vision transformers. In *Proceedings of the IEEE/CVF International Conference on Computer Vision (ICCV)*, pages 11936–11945, 2021. 6
- [46] Katherine Hermann, Ting Chen, and Simon Kornblith. The origins and prevalence of texture bias in convolutional neural networks. In *Advances in Neural Information Processing Systems (NeurIPS)*, volume 33, pages 19000–19015, 2020. 1, 2
- [47] Elad Hoffer, Tal Ben-Nun, Itay Hubara, Niv Giladi, Torsten Hoefer, and Daniel Soudry. Augment your batch: Improving generalization through instance repetition. In *2020 IEEE/CVF Conference on Computer Vision and Pattern Recognition (CVPR)*, pages 8126–8135, 2020. 15
- [48] Elad Hoffer, Itay Hubara, and Daniel Soudry. Train longer, generalize better: closing the generalization gap in large

- batch training of neural networks. In *Advances in Neural Information Processing Systems (NeurIPS)*, 2017. 18
- [49] Andrew Howard, Mark Sandler, Grace Chu, Liang-Chieh Chen, Bo Chen, Mingxing Tan, Weijun Wang, Yukun Zhu, Ruoming Pang, Vijay Vasudevan, et al. Searching for mobilenetv3. In *Proceedings of the IEEE/CVF international conference on computer vision (ICCV)*, pages 1314–1324, 2019. 6, 8
- [50] Andrew G. Howard, Menglong Zhu, Bo Chen, Dmitry Kalenichenko, Weijun Wang, Tobias Weyand, Marco Andreetto, and Hartwig Adam. Mobilenets: Efficient convolutional neural networks for mobile vision applications. *ArXiv*, abs/1704.04861, 2017. 3, 8
- [51] Jie Hu, Li Shen, and Gang Sun. Squeeze-and-excitation networks. In *Proceedings of the IEEE/CVF Conference on Computer Vision and Pattern Recognition (CVPR)*, pages 7132–7141, 2018. 1, 2, 3, 5, 7, 8, 19
- [52] Weizhe Hua, Zihang Dai, Hanxiao Liu, and Quoc V. Le. Transformer quality in linear time. In *Proceedings of the International Conference on Machine Learning (ICML)*, 2022. 1, 2, 17
- [53] Gao Huang, Yu Sun, Zhuang Liu, Daniel Sedra, and Kilian Q. Weinberger. Deep networks with stochastic depth. In *Proceedings of the European Conference on Computer Vision (ECCV)*, 2016. 15
- [54] Sergey Ioffe and Christian Szegedy. Batch normalization: Accelerating deep network training by reducing internal covariate shift. In *Proceedings of the International Conference on Machine Learning (ICML)*, pages 448–456. PMLR, 2015. 2
- [55] Sergey Ioffe and Christian Szegedy. Batch normalization: Accelerating deep network training by reducing internal covariate shift. In *Advances in Neural Information Processing Systems (NeurIPS)*, 2015. 17
- [56] Yifan Jiang, Shiyu Chang, and Zhangyang Wang. Transgan: Two pure transformers can make one strong gan, and that can scale up. In *Advances in Neural Information Processing Systems (NeurIPS)*, 2021. 1, 8
- [57] Zihang Jiang, Qibin Hou, Li Yuan, Daquan Zhou, Yujun Shi, Xiaojie Jin, Anran Wang, and Jiashi Feng. All tokens matter: Token labeling for training better vision transformers. In *Advances in Neural Information Processing Systems (NeurIPS)*, 2021. 8
- [58] Alexander Kirillov, Ross B. Girshick, Kaiming He, and Piotr Dollár. Panoptic feature pyramid networks. In *2019 IEEE/CVF Conference on Computer Vision and Pattern Recognition (CVPR)*, pages 6392–6401, 2019. 1, 4, 7, 16
- [59] Alex Krizhevsky, Ilya Sutskever, and Geoffrey E. Hinton. Imagenet classification with deep convolutional neural networks. *Communications of the ACM*, 60:84 – 90, 2012. 1, 8
- [60] Yann LeCun, Léon Bottou, Yoshua Bengio, and Patrick Haffner. Gradient-based learning applied to document recognition. *Proceedings of the IEEE*, 86(11):2278–2324, 1998. 1, 8
- [61] Kunchang Li, Yali Wang, Junhao Zhang, Peng Gao, Guanglu Song, Yu Liu, Hongsheng Li, and Yu Qiao. Uniformer: Unifying convolution and self-attention for visual recognition. In *International Conference on Learning Representations (ICLR)*, 2022. 1, 4, 5, 6, 7, 8, 16
- [62] Siyuan Li, Zicheng Liu, Di Wu, Zihan Liu, and Stan Z. Li. Boosting discriminative visual representation learning with scenario-agnostic mixup. *ArXiv*, abs/2111.15454, 2021. 15
- [63] Siyuan Li, Zedong Wang, Zicheng Liu, Di Wu, and Stan Z. Li. Openmixup: Open mixup toolbox and benchmark for visual representation learning. <https://github.com/Westlake-AI/openmixup>, 2022. 15
- [64] Siyuan Li, Di Wu, Fang Wu, Zelin Zang, Kai Wang, Lei Shang, Baigui Sun, Haoyang Li, and Stan Z. Li. Architecture-agnostic masked image modeling - from vit back to cnn. *ArXiv*, abs/2205.13943, 2022. 4, 8
- [65] Yunsheng Li, Yinpeng Chen, Xiyang Dai, Dongdong Chen, Mengchen Liu, Lu Yuan, Zicheng Liu, Lei Zhang, and Nuno Vasconcelos. Micronet: Improving image recognition with extremely low flops. In *Proceedings of the IEEE/CVF International Conference on Computer Vision (ICCV)*, pages 468–477, 2021. 6, 7
- [66] Yanyu Li, Geng Yuan, Yang Wen, Eric Hu, Georgios Evangelidis, S. Tulyakov, Yanzhi Wang, and Jian Ren. Efficientformer: Vision transformers at mobilenet speed. In *Advances in Neural Information Processing Systems (NeurIPS)*, 2022. 5, 6, 8
- [67] Mingbao Lin, Mengzhao Chen, Yu xin Zhang, Ke Li, Yunhang Shen, Chunhua Shen, and Rongrong Ji. Super vision transformer. *ArXiv*, abs/2205.11397, 2022. 8
- [68] Tsung-Yi Lin, Piotr Dollár, Ross B. Girshick, Kaiming He, Bharath Hariharan, and Serge J. Belongie. Feature pyramid networks for object detection. *2017 IEEE Conference on Computer Vision and Pattern Recognition (CVPR)*, pages 936–944, 2017. 4
- [69] Tsung-Yi Lin, Michael Maire, Serge Belongie, James Hays, Pietro Perona, Deva Ramanan, Piotr Dollár, and C Lawrence Zitnick. Microsoft coco: Common objects in context. In *Proceedings of the European Conference on Computer Vision (ECCV)*, pages 740–755. Springer, 2014. 6, 16
- [70] S. Liu, Tianlong Chen, Xiaohan Chen, Xuxi Chen, Qiao Xiao, Boqian Wu, Mykola Pechenizkiy, Decebal Constantin Mocanu, and Zhangyang Wang. More convnets in the 2020s: Scaling up kernels beyond 51x51 using sparsity. *ArXiv*, abs/2207.03620, 2022. 6, 7, 8
- [71] Zicheng Liu, Siyuan Li, Ge Wang, Cheng Tan, Lirong Wu, and Stan Z. Li. Decoupled mixup for data-efficient learning. *ArXiv*, abs/2203.10761, 2022. 15
- [72] Zicheng Liu, Siyuan Li, Di Wu, Zhiyuan Chen, Lirong Wu, Jianzhu Guo, and Stan Z. Li. Automix: Unveiling the power of mixup for stronger classifiers. In *Proceedings of the European Conference on Computer Vision (ECCV)*, 2022. 15
- [73] Ze Liu, Yutong Lin, Yue Cao, Han Hu, Yixuan Wei, Zheng Zhang, Stephen Lin, and Baining Guo. Swin transformer: Hierarchical vision transformer using shifted windows. In *International Conference on Computer Vision (ICCV)*, 2021. 1, 2, 5, 6, 7, 8, 15, 16, 17, 19
- [74] Zhuang Liu, Hanzi Mao, Chao-Yuan Wu, Christoph Feichtenhofer, Trevor Darrell, and Saining Xie. A convnet for

- the 2020s. In *Proceedings of the IEEE/CVF Conference on Computer Vision and Pattern Recognition (CVPR)*, pages 11976–11986, 2022. [1](#), [2](#), [5](#), [6](#), [7](#), [8](#), [15](#), [16](#), [17](#), [18](#), [19](#)
- [75] Ze Liu, Jia Ning, Yue Cao, Yixuan Wei, Zheng Zhang, Stephen Lin, and Han Hu. Video swin transformer. In *2022 IEEE/CVF Conference on Computer Vision and Pattern Recognition (CVPR)*, pages 3192–3201, 2022. [1](#)
- [76] Ilya Loshchilov and Frank Hutter. Sgdr: Stochastic gradient descent with warm restarts. *arXiv preprint arXiv:1608.03983*, 2016. [6](#), [15](#)
- [77] Ilya Loshchilov and Frank Hutter. Decoupled weight decay regularization. In *International Conference on Learning Representations (ICLR)*, 2019. [6](#), [15](#), [16](#)
- [78] Jiachen Lu, Jinghan Yao, Junge Zhang, Xiatian Zhu, Hang Xu, Weiguo Gao, Chunjing Xu, Tao Xiang, and Li Zhang. Soft: Softmax-free transformer with linear complexity. In *Advances in Neural Information Processing Systems (NeurIPS)*, 2021. [3](#)
- [79] Wenjie Luo, Yujia Li, Raquel Urtasun, and Richard S. Zemel. Understanding the effective receptive field in deep convolutional neural networks. *ArXiv*, abs/1701.04128, 2016. [1](#), [8](#)
- [80] Ningning Ma, Xiangyu Zhang, Hai-Tao Zheng, and Jian Sun. Shufflenet v2: Practical guidelines for efficient cnn architecture design. In *Proceedings of the European conference on computer vision (ECCV)*, pages 116–131, 2018. [6](#), [8](#)
- [81] Sachin Mehta and Mohammad Rastegari. Mobilevit: lightweight, general-purpose, and mobile-friendly vision transformer. In *International Conference on Learning Representations (ICLR)*, 2022. [6](#), [8](#), [15](#)
- [82] Muhammad Muzammal Naseer, Kanchana Ranasinghe, Salman H Khan, Munawar Hayat, Fahad Shahbaz Khan, and Ming-Hsuan Yang. Intriguing properties of vision transformers. In *Advances in Neural Information Processing Systems (NeurIPS)*, 2021. [3](#)
- [83] Zizheng Pan, Jianfei Cai, and Bohan Zhuang. Fast vision transformers with hilo attention. In *Advances in Neural Information Processing Systems (NeurIPS)*, 2022. [3](#), [4](#), [5](#), [6](#), [7](#), [8](#), [17](#)
- [84] Zizheng Pan, Bohan Zhuang, Haoyu He, Jing Liu, and Jianfei Cai. Less is more: Pay less attention in vision transformers. In *Proceedings of the AAAI Conference on Artificial Intelligence (AAAI)*, 2022. [5](#), [8](#)
- [85] Namuk Park and Songkuk Kim. How do vision transformers work? In *International Conference on Learning Representations (ICLR)*, 2022. [2](#), [3](#), [4](#)
- [86] Niki Parmar, Ashish Vaswani, Jakob Uszkoreit, Lukasz Kaiser, Noam Shazeer, Alexander Ku, and Dustin Tran. Image transformer. In *Proceedings of the International Conference on Machine Learning (ICML)*, 2018. [8](#)
- [87] Francesco Pinto, Philip HS Torr, and Puneet K Dokania. An impartial take to the cnn vs transformer robustness contest. *Proceedings of the European Conference on Computer Vision (ECCV)*, 2022. [1](#), [2](#), [4](#)
- [88] Boris Polyak and Anatoli B. Juditsky. Acceleration of stochastic approximation by averaging. *Siam Journal on Control and Optimization*, 30:838–855, 1992. [15](#)
- [89] Zhen Qin, Weixuan Sun, Huicai Deng, Dongxu Li, Yunshen Wei, Baohong Lv, Junjie Yan, Lingpeng Kong, and Yiran Zhong. cosformer: Rethinking softmax in attention. In *International Conference on Learning Representations (ICLR)*, 2022. [3](#)
- [90] Ilija Radosavovic, Raj Prateek Kosaraju, Ross B. Girshick, Kaiming He, and Piotr Dollár. Designing network design spaces. In *2020 IEEE/CVF Conference on Computer Vision and Pattern Recognition (CVPR)*, pages 10425–10433, 2020. [1](#), [5](#), [6](#), [7](#), [8](#), [19](#)
- [91] Maithra Raghu, Thomas Unterthiner, Simon Kornblith, Chiyuan Zhang, and Alexey Dosovitskiy. Do vision transformers see like convolutional neural networks? *Advances in Neural Information Processing Systems (NeurIPS)*, 34:12116–12128, 2021. [2](#)
- [92] Yongming Rao, Wenliang Zhao, Yansong Tang, Jie Zhou, Ser Nam Lim, and Jiwen Lu. Hornet: Efficient high-order spatial interactions with recursive gated convolutions. In *Advances in Neural Information Processing Systems (NeurIPS)*, 2022. [4](#), [6](#), [7](#), [8](#), [17](#)
- [93] Shaoqing Ren, Kaiming He, Ross B. Girshick, and Jian Sun. Faster r-cnn: Towards real-time object detection with region proposal networks. *IEEE Transactions on Pattern Analysis and Machine Intelligence (TPAMI)*, 39:1137–1149, 2015. [1](#), [4](#)
- [94] Mark Sandler, Andrew G. Howard, Menglong Zhu, Andrey Zhmoginov, and Liang-Chieh Chen. Mobilenetv2: Inverted residuals and linear bottlenecks. In *Proceedings of the IEEE/CVF Conference on Computer Vision and Pattern Recognition (CVPR)*, pages 4510–4520, 2018. [2](#), [3](#), [8](#)
- [95] Ramprasaath R Selvaraju, Michael Cogswell, Abhishek Das, Ramakrishna Vedantam, Devi Parikh, and Dhruv Batra. Grad-cam: Visual explanations from deep networks via gradient-based localization. In *Proceedings of the IEEE international conference on computer vision (CVPR)*, pages 618–626, 2017. [8](#), [17](#)
- [96] Noam M. Shazeer. Glu variants improve transformer. *ArXiv*, abs/2002.05202, 2020. [3](#), [17](#)
- [97] Zhiqiang Shen, Zechun Liu, and Eric Xing. Sliced recursive transformer. In *Proceedings of the European Conference on Computer Vision (ECCV)*, 2022. [6](#)
- [98] Chenyang Si, Weihao Yu, Pan Zhou, Yichen Zhou, Xinchao Wang, and Shuicheng Yan. Inception transformer. In *Advances in Neural Information Processing Systems (NeurIPS)*, 2022. [4](#), [8](#), [17](#)
- [99] Laurent Sifre and Stéphane Mallat. Rigid-motion scattering for texture classification. *arXiv preprint arXiv:1403.1687*, 2014. [1](#)
- [100] Karen Simonyan and Andrew Zisserman. Very deep convolutional networks for large-scale image recognition. *arXiv preprint arXiv:1409.1556*, 2014. [3](#)
- [101] A. Srinivas, Tsung-Yi Lin, Niki Parmar, Jonathon Shlens, P. Abbeel, and Ashish Vaswani. Bottleneck transformers for visual recognition. *2021 IEEE/CVF Conference on Computer Vision and Pattern Recognition (CVPR)*, pages 16514–16524, 2021. [7](#)
- [102] Christian Szegedy, Vincent Vanhoucke, Sergey Ioffe, Jonathon Shlens, and Zbigniew Wojna. Rethinking the

- inception architecture for computer vision. *2016 IEEE Conference on Computer Vision and Pattern Recognition (CVPR)*, pages 2818–2826, 2016. 3, 15
- [103] Mingxing Tan and Quoc Le. Efficientnet: Rethinking model scaling for convolutional neural networks. In *International conference on machine learning (ICML)*, pages 6105–6114. PMLR, 2019. 3, 5, 6, 7, 8, 19
- [104] Mingxing Tan and Quoc V. Le. Efficientnetv2: Smaller models and faster training. In *International conference on machine learning (ICML)*, 2021. 19
- [105] Ilya O. Tolstikhin, Neil Houlsby, Alexander Kolesnikov, Lucas Beyer, Xiaohua Zhai, Thomas Unterthiner, Jessica Yung, Daniel Keysers, Jakob Uszkoreit, Mario Lucic, and Alexey Dosovitskiy. Mlp-mixer: An all-mlp architecture for vision. In *Advances in Neural Information Processing Systems (NeurIPS)*, 2021. 2, 3, 5, 8
- [106] Hugo Touvron, Matthieu Cord, Matthijs Douze, Francisco Massa, Alexandre Sablayrolles, and Herve Jegou. Training data-efficient image transformers & distillation through attention. In *International Conference on Machine Learning (ICML)*, pages 10347–10357, 2021. 1, 6, 7, 8, 15, 17, 18, 19
- [107] Hugo Touvron, Matthieu Cord, Matthijs Douze, Francisco Massa, Alexandre Sablayrolles, and Hervé Jégou. Training data-efficient image transformers & distillation through attention. In *Proceedings of the International Conference on Machine Learning (ICML)*, 2021. 8
- [108] Hugo Touvron, Matthieu Cord, Alaaeldin El-Nouby, Piotr Bojanowski, Armand Joulin, Gabriel Synnaeve, Jakob Verbeek, and Hervé Jégou. Augmenting convolutional networks with attention-based aggregation. *arXiv preprint arXiv:2112.13692*, 2021. 5
- [109] Hugo Touvron, Matthieu Cord, and Hervé Jégou. Deit iii: Revenge of the vit. In *Proceedings of the European Conference on Computer Vision (ECCV)*, 2022. 6, 8, 18
- [110] Anne M Treisman and Garry Gelade. A feature-integration theory of attention. *Cognitive psychology*, 12(1):97–136, 1980. 2, 4
- [111] Asher Trockman and J. Zico Kolter. Patches are all you need? *ArXiv*, abs/2201.09792, 2022. 2, 8
- [112] Shikhar Tuli, Ishita Dasgupta, Erin Grant, and Thomas L. Griffiths. Are convolutional neural networks or transformers more like human vision? *ArXiv*, abs/2105.07197, 2021. 1, 4
- [113] Ashish Vaswani, Noam Shazeer, Niki Parmar, Jakob Uszkoreit, Llion Jones, Aidan N Gomez, Łukasz Kaiser, and Illia Polosukhin. Attention is all you need. In *Advances in Neural Information Processing Systems (NeurIPS)*, 2017. 1, 2, 3, 8
- [114] Guangting Wang, Yucheng Zhao, Chuanxin Tang, Chong Luo, and Wenjun Zeng. When shift operation meets vision transformer: An extremely simple alternative to attention mechanism. In *Proceedings of the AAAI Conference on Artificial Intelligence (AAAI)*, 2022. 3, 8
- [115] Jiayun Wang, Yubei Chen, Rudrasis Chakraborty, and Stella X. Yu. Orthogonal convolutional neural networks. In *2020 IEEE/CVF Conference on Computer Vision and Pattern Recognition (CVPR)*, pages 11502–11512, 2020. 5
- [116] Peihao Wang, Wenqing Zheng, Tianlong Chen, and Zhangyang Wang. Anti-oversmoothing in deep vision transformers via the fourier domain analysis: From theory to practice. *International Conference on Learning Representations (ICLR)*, 2022. 4
- [117] Qiang Wang, Bei Li, Tong Xiao, Jingbo Zhu, Changliang Li, Derek F. Wong, and Lidia S. Chao. Learning deep transformer models for machine translation. In *Annual Meeting of the Association for Computational Linguistics (ACL)*, 2019. 2
- [118] Sinong Wang, Belinda Z. Li, Madian Khabsa, Han Fang, and Hao Ma. Linformer: Self-attention with linear complexity. In *Advances in Neural Information Processing Systems (NeurIPS)*, 2021. 1, 3, 8
- [119] Wenhai Wang, Enze Xie, Xiang Li, Deng-Ping Fan, Kaitao Song, Ding Liang, Tong Lu, Ping Luo, and Ling Shao. Pyramid vision transformer: A versatile backbone for dense prediction without convolutions. In *2021 IEEE/CVF International Conference on Computer Vision (ICCV)*, pages 548–558, 2021. 1, 2, 6, 8
- [120] Wenhai Wang, Enze Xie, Xiang Li, Deng-Ping Fan, Kaitao Song, Ding Liang, Tong Lu, Ping Luo, and Ling Shao. Pvtv2: Improved baselines with pyramid vision transformer. *Computational Visual Media (CVMJ)*, 2022. 5
- [121] Xiaolong Wang, Ross Girshick, Abhinav Gupta, and Kaiming He. Non-local neural networks. In *Proceedings of the IEEE/CVF Conference on Computer Vision and Pattern Recognition (CVPR)*, pages 7794–7803, 2018. 1, 3, 8
- [122] Ross Wightman, Hugo Touvron, and Hervé Jégou. Resnet strikes back: An improved training procedure in timm, 2021. 2, 6, 15, 18, 19
- [123] Sanghyun Woo, Jongchan Park, Joon-Young Lee, and In-So Kweon. Cbam: Convolutional block attention module. In *Proceedings of the European Conference on Computer Vision (ECCV)*, 2018. 1, 5, 8
- [124] Fang Wu, Siyuan Li, Lirong Wu, Stan Z Li, Dragomir Radev, and Qiang Zhang. Discovering the representation bottleneck of graph neural networks from multi-order interactions. *arXiv preprint arXiv:2205.07266*, 2022. 2
- [125] Haixu Wu, Jialong Wu, Jiehui Xu, Jianmin Wang, and Mingsheng Long. Flowformer: Linearizing transformers with conservation flows. In *Proceedings of the International Conference on Machine Learning (ICML)*, 2022. 1, 3
- [126] Haiping Wu, Bin Xiao, Noel Codella, Mengchen Liu, Xiyang Dai, Lu Yuan, and Lei Zhang. Cvt: Introducing convolutions to vision transformers. *Proceedings of the IEEE/CVF International Conference on Computer Vision (ICCV)*, 2021. 1, 8
- [127] Kan Wu, Houwen Peng, Minghao Chen, Jianlong Fu, and Hongyang Chao. Rethinking and improving relative position encoding for vision transformer. In *Proceedings of the IEEE/CVF International Conference on Computer Vision (ICCV)*, pages 10033–10041, 2021. 8
- [128] Kan Wu, Jinnian Zhang, Houwen Peng, Mengchen Liu, Bin Xiao, Jianlong Fu, and Lu Yuan. Tinyvit: Fast pretraining distillation for small vision transformers. In *Proceedings*

- of the European Conference on Computer Vision (ECCV), 2022. 8
- [129] Yuxin Wu and Justin Johnson. Rethinking "batch" in batch-norm. *ArXiv*, abs/2105.07576, 2021. 17, 18
- [130] Tete Xiao, Yingcheng Liu, Bolei Zhou, Yuning Jiang, and Jian Sun. Unified perceptual parsing for scene understanding. In *European Conference on Computer Vision (ECCV)*. Springer, 2018. 4, 7, 16
- [131] Tete Xiao, Mannat Singh, Eric Mintun, Trevor Darrell, Piotr Dollár, and Ross B. Girshick. Early convolutions help transformers see better. In *Advances in Neural Information Processing Systems (NeurIPS)*, 2021. 6, 8
- [132] Saining Xie, Ross Girshick, Piotr Dollár, Zhuowen Tu, and Kai Ming He. Aggregated residual transformations for deep neural networks. In *Proceedings of the IEEE/CVF Conference on Computer Vision and Pattern Recognition (CVPR)*, pages 1492–1500, 2017. 1, 2, 3, 8, 19
- [133] Yufei Xu, Qiming Zhang, Jing Zhang, and Dacheng Tao. Vitae: Vision transformer advanced by exploring intrinsic inductive bias. *Advances in Neural Information Processing Systems (NeurIPS)*, 34, 2021. 6
- [134] Daniel LK Yamins, Ha Hong, Charles F Cadieu, Ethan A Solomon, Darren Seibert, and James J DiCarlo. Performance-optimized hierarchical models predict neural responses in higher visual cortex. *Proceedings of the national academy of sciences*, 111(23):8619–8624, 2014. 1
- [135] Jianwei Yang, Chunyuan Li, Xiyang Dai, and Jianfeng Gao. Focal modulation networks. In *Advances in Neural Information Processing Systems (NeurIPS)*, 2022. 7, 8
- [136] Jianwei Yang, Chunyuan Li, Pengchuan Zhang, Xiyang Dai, Bin Xiao, Lu Yuan, and Jianfeng Gao. Focal self-attention for local-global interactions in vision transformers. *ArXiv*, abs/2107.00641, 2021. 7, 8
- [137] Yang You, Jing Li, Sashank Reddi, Jonathan Hseu, Sanjiv Kumar, Srinadh Bhojanapalli, Xiaodan Song, James Demmel, Kurt Keutzer, and Cho-Jui Hsieh. Large batch optimization for deep learning: Training BERT in 76 minutes. In *International Conference on Learning Representations (ICLR)*, 2020. 18
- [138] Fisher Yu and Vladlen Koltun. Multi-scale context aggregation by dilated convolutions. In *International Conference on Learning Representations (ICLR)*, 2016. 3
- [139] Weihao Yu, Mi Luo, Pan Zhou, Chenyang Si, Yichen Zhou, Xinchao Wang, Jiashi Feng, and Shuicheng Yan. Metaformer is actually what you need for vision. In *Proceedings of the IEEE/CVF Conference on Computer Vision and Pattern Recognition (CVPR)*, pages 10819–10829, 2022. 2, 3, 7, 8, 15, 16, 18
- [140] Li Yuan, Yunpeng Chen, Tao Wang, Weihao Yu, Yujun Shi, Zihang Jiang, Francis EH Tay, Jiashi Feng, and Shuicheng Yan. Tokens-to-token vit: Training vision transformers from scratch on imagenet. In *International Conference on Computer Vision (ICCV)*, 2021. 8
- [141] Li Yuan, Yunpeng Chen, Tao Wang, Weihao Yu, Yujun Shi, Francis E. H. Tay, Jiashi Feng, and Shuicheng Yan. Tokens-to-token vit: Training vision transformers from scratch on imagenet. *2021 IEEE/CVF International Conference on Computer Vision (ICCV)*, pages 538–547, 2021. 6, 7, 15, 17
- [142] Sangdoo Yun, Dongyoon Han, Seong Joon Oh, Sanghyuk Chun, Junsuk Choe, and Youngjoon Yoo. Cutmix: Regularization strategy to train strong classifiers with localizable features. In *Proceedings of the IEEE/CVF International Conference on Computer Vision (ICCV)*, pages 6023–6032, 2019. 15
- [143] Sergey Zagoruyko and Nikos Komodakis. Wide residual networks. In *Proceedings of the British Machine Vision Conference (BMVC)*, 2016. 8
- [144] Hongyi Zhang, Moustapha Cisse, Yann N Dauphin, and David Lopez-Paz. mixup: Beyond empirical risk minimization. In *International Conference on Learning Representations (ICLR)*, 2018. 15
- [145] Haokui Zhang, Wenzhe Hu, and Xiaoyu Wang. Edgeformer: Improving light-weight convnets by learning from vision transformers. In *Proceedings of the European Conference on Computer Vision (ECCV)*, 2022. 2, 4, 6, 15, 18
- [146] Hao Zhang, Sen Li, Yinchao Ma, Mingjie Li, Yichen Xie, and Quanshi Zhang. Interpreting and boosting dropout from a game-theoretic view. *arXiv preprint arXiv:2009.11729*, 2020. 4
- [147] Hang Zhang, Chongruo Wu, Zhongyue Zhang, Yi Zhu, Haibin Lin, Zhi Zhang, Yue Sun, Tong He, Jonas Mueller, R Manmatha, et al. Resnest: Split-attention networks. In *Proceedings of the IEEE/CVF Conference on Computer Vision and Pattern Recognition (CVPR)*, pages 2736–2746, 2022. 1, 8
- [148] Zhun Zhong, Liang Zheng, Guoliang Kang, Shaozi Li, and Yi Yang. Random erasing data augmentation. In *Proceedings of the AAAI conference on artificial intelligence (AAAI)*, pages 13001–13008, 2020. 15
- [149] Bolei Zhou, Hang Zhao, Xavier Puig, Sanja Fidler, Adela Barriuso, and Antonio Torralba. Semantic understanding of scenes through the ade20k dataset. *International Journal of Computer Vision (IJCV)*, 127:302–321, 2018. 6, 16
- [150] Daquan Zhou, Zhiding Yu, Enze Xie, Chaowei Xiao, Anima Anandkumar, Jiashi Feng, and José Manuel Álvarez. Understanding the robustness in vision transformers. In *Proceedings of the International Conference on Machine Learning (ICML)*, 2022. 3, 7
- [151] Xizhou Zhu, Weiye Su, Lewei Lu, Bin Li, Xiaogang Wang, and Jifeng Dai. Deformable detr: Deformable transformers for end-to-end object detection. In *International Conference on Learning Representations (ICLR)*, 2021. 1, 8

A. Implementation Details

A.1. Architecture Details

The detailed architecture specifications of MogaNet are shown in Table A1 and Figure A1, where an input image size of 224^2 is assumed for all architectures. We rescale the groups of embedding dimensions the number of Moga Blocks for each stage corresponding to different models of varying magnitudes: i) MogaNet-X-Tiny and MogaNet-Tiny with embedding dimensions of $\{32, 64, 96, 192\}$ and $\{32, 64, 128, 256\}$ has the competitive computational overload as recently proposed light-weight architectures [16, 81, 145]; ii) MogaNet-Small adopts embedding dimensions of $\{64, 128, 320, 512\}$ in comparison to small-scale architectures [73, 74]; iii) MogaNet-Base with embedding dimensions of $\{64, 160, 320, 512\}$ in comparison to medium size architectures; iv) MogaNet-Large with embedding dimensions of $\{64, 160, 320, 640\}$ is designed for large-scale computer vision tasks. The FLOPs are measured for image classification on ImageNet [27] at resolution 224^2 , where a global average pooling (GAP) layer is applied to the output feature map of the last stage, followed by a linear classifier.

Stage	Output Size	Layer Settings	MogaNet				
			X-Tiny	Tiny	Small	Base	Large
Stage 1	$\frac{H}{4} \times \frac{W}{4}$	Stem	Conv _{3×3} , stride 2, C/2				
			Conv _{3×3} , stride 2, C				
		Embed. Dim.	32	32	64	64	64
		# Moga Block	3	3	2	4	4
		MLP Ratio	8				
Stage 2	$\frac{H}{8} \times \frac{W}{8}$	Stem	Conv _{3×3} , stride 2				
		Embed. Dim.	64	64	128	160	160
		# Moga Block	3	3	3	6	6
		MLP Ratio	8				
Stage 3	$\frac{H}{16} \times \frac{W}{16}$	Stem	Conv _{3×3} , stride 2				
		Embed. Dim.	96	128	320	320	320
		# Moga Block	10	12	12	22	44
		MLP Ratio	4				
Stage 4	$\frac{H}{32} \times \frac{W}{32}$	Stem	Conv _{3×3} , stride 2				
		Embed. Dim.	192	256	512	512	640
		# Moga Block	2	2	2	3	4
		MLP Ratio	4				
Classifier			Global Average Pooling, Linear				
Parameters (M)			2.97	5.20	25.3	43.8	82.5
FLOPs (G)			0.80	1.10	4.97	9.93	15.9

Table A1. Architecture configurations of the variants of MogaNet.

A.2. Experimental Settings for ImageNet-1K

We perform regular ImageNet-1K training mostly following the training settings of DeiT [106] and RSB A2 [122] in Table A2, which are widely adopted for Transformer and ConvNet models. For all models, the default input image resolution is 224^2 for training from scratch. We adopt 256^2 resolutions for lightweight experiments according to MobileViT [81]. Taking training settings for the

model with 25M or more parameters as the default, we train all MogaNet models for 300 epochs by AdamW [77] optimizer using a batch size of 1024, a basic learning rate of 1×10^{-3} , a weight decay of 0.05, and a Cosine learning rate scheduler [76] with 5 epochs of linear warmup [28]. As for augmentation and regularization techniques, we adopt most of the data augmentation and regularization strategies applied in DeiT training settings, including RandAugment [21], Mixup [144], CutMix [142], random erasing [148], stochastic depth [53], and label smoothing [102]. Similar to ConvNeXt [74], we do not apply Repeated augmentation [47] and gradient clipping, which are designed for Transformers but do not enhance the performances of ConvNets, while using Exponential Moving Average (EMA) [88] with the decay rate of 0.9999 by default. We also remove additional augmentation strategies [20, 62, 71, 72] for ConvNets, *e.g.*, ColorJitter [42] and AutoAugment [20]. Since lightweight architectures (3~10M parameters) tend to get under-fitted with strong augmentations and regularization, we adjust the training configurations for MogaNet-XT/T following [16, 81, 145], including employing the weight decay of 0.03 and 0.04, Mixup with α of 0.1, and RandAugment of 7/0.5 for MogaNet-XT/T. Since EMA is proposed to stabilize the training process of large models, we also remove it for MogaNet-XT/T as a fair comparison. An increasing degree of stochastic depth path augmentation is employed for larger models, *i.e.*, 0.05, 0.1, 0.1, 0.2, 0.3 for MogaNet-XT, MogaNet-T, MogaNet-S, MogaNet-B, MogaNet-L, respectively. In evaluation, the top-1 accuracy using a single crop with a test crop ratio of 0.9 is reported as [37, 139, 141]. All experiments are implemented on OpenMixup [63] codebase.

Configuration	DeiT	RSB A2	MogaNet				
			X-Tiny	Tiny	Small	Base	Large
Input resolution	224^2	224^2	224^2				
Epochs	300	300	300				
Batch size	1024	2048	1024				
Optimizer	AdamW	LAMB	AdamW				
AdamW (β_1, β_2)	(0.9, 0.999)	-	(0.9, 0.999)				
Learning rate	1×10^{-3}	5×10^{-3}	1×10^{-3}				
Learning rate decay	Cosine	Cosine	Cosine				
Weight decay	0.05	0.02	0.03	0.04	0.05	0.05	0.05
Warmup epochs	5	5	5				
Label smoothing ϵ	0.1	0.1	0.1				
Stochastic Depth	✓	✓	0.05	0.1	0.1	0.2	0.3
Rand Augment	9/0.5	7/0.5	7/0.5	7/0.5	9/0.5	9/0.5	9/0.5
Repeated Aug	✓	✓	✗				
Mixup α	0.8	0.1	0.1	0.1	0.8	0.8	0.8
CutMix α	1.0	1.0	1.0				
Erasing prob.	0.25	✗	0.25				
ColorJitter	✗	✗	✗				
Gradient Clipping	✓	✗	✗				
EMA decay	✓	✗	✗	✗	✓	✓	✓
Test crop ratio	0.875	0.95	0.90				

Table A2. Hyper-parameters for ImageNet-1K training of DeiT, RSB A2, and MogaNet.

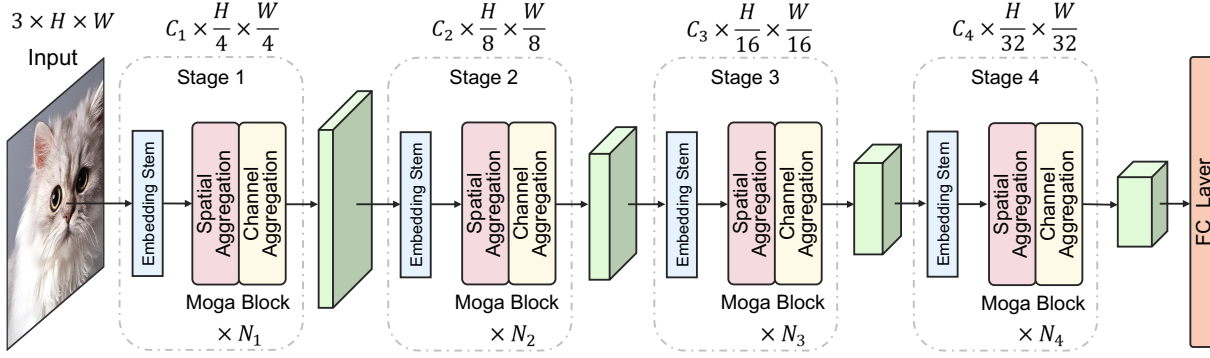


Figure A1. **The overall framework of MogaNet.** Similar to [42, 73, 74, 139], MogaNet uses hierarchical architectures of 4 stages. The stage i consists of an embedding stem and N_i Moga Blocks, which contain spatial aggregation blocks and channel aggregation blocks.

A.3. Object Detection and Segmentation on COCO

Following Swin [73] and PoolFormer [139], we evaluate objection detection and instance segmentation tasks on COCO [69] benchmark, which include 118K training images (*train2017*) and 5K validation images (*val2017*). We adopt Mask-RCNN [41] as the standard detectors and use ImageNet-1K pre-trained weights as the initialization of the backbones. We employ AdamW [77] optimizer for training $1 \times$ schedulers (12-epochs) with a basic learning rate of 1×10^{-4} and a batch size of 16. The shorter side of training images is resized to 800 pixels, and the longer side is resized to not more than 1333 pixels. We calculate the FLOPs of compared models at 800×1280 resolutions. Experiments of COCO are implemented on MMDetection [14] codebase and run on 8 NVIDIA A100 GPUs.

A.4. Semantic Segmentation on ADE20K

We evaluate semantic segmentation on ADE20K [149] benchmark, which contains 20K training images and 2K validation images, covering 150 fine-grained semantic categories. We first adopt Semantic FPN [58] following PoolFormer [139] and Uniformer [61], which train models for 80K iterations by AdamW [77] optimizer with a basic learning rate of 2×10^{-4} and a batch size of 16. Then, we utilize UperNet [130] following Swin [73], which employs AdamW optimizer using a basic learning rate of 6×10^{-5} , a weight decay of 0.01, a linear learning rate scheduler with a linear warmup of 1,500 iterations. We use ImageNet-1K pre-trained weights as the initialization of the backbones. The training images are resized to 512² resolutions, and the shorter side of testing images is resized to 512 pixels. We calculate the FLOPs of models at 800×2048 resolutions. The pre-trained weights on ImageNet-1K are used as the initialization of backbones. Experiments of ADE20K are implemented on MMSegmentation [19] codebase and run on 8 NVIDIA A100 GPUs.

B. Empirical Experiment Results

B.1. Multi-order Interaction

In Sec. 3, we interpret the learned representation of backbones by multi-order interaction [26]. The interaction complexity can be represented by the multi-order interaction $I^{(m)}(i, j)$, which measures the average interaction utility between variables i, j on all contexts consisting of m variables. Empirically, the m -th order interaction $I^{(m)}(i, j)$ is defined to be the average interaction utility between image patches i and j on all contexts consisting of m image patches. Note that m denotes the order of contextual complexity of the interaction. Formally, given an input image x with a set of n patches $N = \{1, \dots, n\}$ (e.g., an image with n pixels in total), the multi-order interaction $I^{(m)}(i, j)$ can be calculated as:

$$I^{(m)}(i, j) = \mathbb{E}_{S \subseteq N \setminus \{i, j\}, |S|=m} [\Delta f(i, j, S)], \quad (11)$$

where $\Delta f(i, j, S) = f(S \cup \{i, j\}) - f(S \cup \{i\}) - f(S \cup \{j\}) + f(S)$. $f(S)$ indicates the score of output with patches in $N \setminus S$ kept unchanged but replaced with the baseline value [1], where the context $S \subseteq N$. Notice that the order m reflects the contextual complexity of the interaction $I^{(m)}(i, j)$. For example, a low-order interaction (e.g., $m = 0.05n$) means the relatively simple collaboration between variables i, j , while a high-order interaction (e.g., $m = 0.05n$) corresponds to the complex collaboration. Then, we can measure the overall interaction complexity of deep neural networks (DNNs) by the relative interaction strength $J^{(m)}$ of the encoded m -th order interaction:

$$J^{(m)} = \frac{\mathbb{E}_{x \in \Omega} \mathbb{E}_{i, j} |I^{(m)}(i, j|x)|}{\mathbb{E}_{m'} \mathbb{E}_{x \in \Omega} \mathbb{E}_{i, j} |I^{(m')}(i, j|x)|}, \quad (12)$$

where Ω is the set of all samples and $0 \leq m \leq n - 2$. Note that $J^{(m)}$ is the average interaction strength over all possible patch pairs of the input samples and indicates the distribution (area under curve sums up to one) of the order of interactions of DNNs. In Figure 3, we calculate the interaction strength $J^{(m)}$ with Eq. 12 for the models trained on

ImageNet-1K using the official implementation¹ provided by [26]. Specially, we use the image of 224×224 resolution as the input and calculate $J^{(m)}$ on 14×14 grids, i.e., $n = 14 \times 14$. And we set the model output as $f(x_S) = \log \frac{P(\hat{y}=y|x_S)}{1-P(\hat{y}=y|x_S)}$ given the masked sample x_S , where y denotes the ground-truth label and $P(\hat{y} = y|x_S)$ denotes the probability of classifying the masked sample x_S to the true category.

B.2. Visualization of CAM

We further visualize more examples of Grad-CAM [95] activation maps of MogaNet-S in comparison to Transformers, including DeiT-S [106], T2T-ViT-S [141], Twins-S [18], and Swin [73], and ConvNets, including ResNet-50 [42] and ConvNeXt-T [74], on ImageNet-1K in Figure A2. Due to the self-attention mechanism, the pure Transformers architectures (DeiT-S and T2T-ViT-S) show more refined activation maps than ConvNets, but they also activate some irrelevant parts. Combined with the design of local windows, local attention architectures (Twins-S and Swin-T) can locate the full semantic objects. Results of previous ConvNets can roughly localize the semantic target but might contain some background regions. The activation parts of our proposed MogaNet-S are more similar to local attention architectures than previous ConvNets, which are more gathered on the semantic objects.

C. More Ablation and Analysis Results

In addition to Sec. 5.3, we further conduct more ablation and analysis of our proposed MogaNet on ImageNet-1K. We adopt the same experimental settings as Sec. 2.

C.1. Ablation of Activation Functions

We conduct the ablation of activation functions used in the proposed multi-order gated aggregation module on ImageNet-1K. Table A3 shows that using SiLU [32] activation for both branches achieves the best performance. Similar results were also found in Transformers, e.g., GLU variants with SiLU or GELU [44] yield better performances than using Sigmoid or Tanh activation functions [52, 96]. We guess that SiLU is the most suitable activation because it has both the property of Sigmoid (gating effects) and GELU (training friendly), which is defined as $x \cdot \text{Sigmoid}(x)$.

C.2. Ablation of Multi-order DWConv Layers

In addition to Sec. 4.2 and Sec. 5.3, we also analyze the multi-order depth-wise convolution (DWConv) layers as the static regionality perception in the multi-order aggregation module Moga(\cdot) on ImageNet-1K. As shown in Table A4, we analyze the channel configuration of three parallel dilated DWConv layers: $\text{DW}_{5 \times 5, d=1}$, $\text{DW}_{5 \times 5, d=2}$,

Top-1	Acc (%)	Context branch		
		None	GELU	SiLU
None		76.3	76.7	76.7
Gating	Sigmoid	76.8	77.0	76.9
branch	GELU	76.7	76.8	77.0
	SiLU	76.9	77.1	77.2

Table A3. Ablation of activation functions for the gating and context branches in the multi-order aggregation module Moga(\cdot).

and $\text{DW}_{7 \times 7, d=3}$ with the channels of C_l , C_m , C_h . we first compare the performance of serial DWConv layers (e.g., $\text{DW}_{5 \times 5, d=1} + \text{DW}_{7 \times 7, d=3}$) and parallel DWConv layers. We find that the parallel design can achieve the same performance with fewer computational overloads because the DWConv kernel is equally applied to all channels. When we adopt three DWConv layers, the proposed parallel design reduces $C_l + C_h$ and $C_l + C_m$ times computations of $\text{DW}_{5 \times 5, d=2}$ and $\text{DW}_{5 \times 5, d=2}$ in comparison to the serial stack of these DWConv layers. Then, we empirically explore the optimal configuration of the three channels. We find that $C_l : C_m : C_h = 1 : 3 : 4$ yields the best performance, which well balances the small, medium, and large DWConv kernels to learn low, middle, and high-order contextual representations. Similar conclusions are also found in relevant designs [83, 92, 98], where global context aggregations take the majority (e.g., $\frac{1}{2} \sim \frac{3}{4}$ channels or context components). We also verify the parallel design with the optimal configuration based on MogaNet-S/B. Therefore, we can conclude that our proposed multi-order DWConv layers can efficiently learn multi-order contextual information for the context branch of Moga(\cdot).

Modules	Top-1	Params.	FLOPs
	Acc (%)	(M)	(G)
Baseline (+Gating branch)	77.2	5.09	1.070
$\text{DW}_{7 \times 7}$	77.4	5.14	1.094
$\text{DW}_{5 \times 5, d=1} + \text{DW}_{7 \times 7, d=3}$	77.5	5.15	1.112
$\text{DW}_{5 \times 5, d=1} + \text{DW}_{5 \times 5, d=2} + \text{DW}_{7 \times 7, d=3}$	77.5	5.17	1.185
+Multi-order, $C_l : C_m : C_h = 1 : 0 : 3$	77.5	5.17	1.099
+Multi-order, $C_l : C_m : C_h = 0 : 1 : 1$	77.6	5.17	1.103
+Multi-order, $C_l : C_m : C_h = 1 : 6 : 9$	77.7	5.17	1.104
+Multi-order, $C_l : C_m : C_h = 1 : 3 : 4$	77.8	5.17	1.102

Table A4. Ablation of multi-order DWConv layers in the proposed Moga(\cdot) module. The baseline adopts the MogaNet framework using the non-linear projection, $\text{DW}_{5 \times 5}$, and the SiLU gating branch as SMixer(\cdot) and using the vanilla MLP as CMixer(\cdot).

C.3. Ablation of Normalization Layers

For most of ConvNets, BatchNorm [55] (BN) is considered an essential component to improve the convergence speed and prevent overfitting. However, BN might cause some instability [129] or harm the final performance of models [7, 8]. Some recently proposed ConvNets [37, 74] replace BN by LayerNorm [3] (LN), which has been widely used in Transformers [31] and Metaformer architec-

¹<https://github.com/Nebularaid2000/bottleneck>

tures [139], achieving relatively good performances in various scenarios. Here, we conduct an ablation of normalization (Norm) layers in MogaNet on ImageNet-1K, as shown in Table A5. As discussed in ConvNeXt [74], the Norm layers used in each block (**within**) and after each stage (**after**) have different effects. Thus we study them separately. Table A5 shows that using BN in both places yields better performance than using LN (after) and BN (within), except MogaNet-T with 224^2 resolutions, while using LN in both places performs the worst. Consequently, we use BN as the default Norm layers in our proposed MogaNet for two reasons: (i) With pure convolution operators, the rule of combining convolution operations with BN within each stage is still useful for modern ConvNets. (ii) Although using LN after each stage might help stabilize the training process of Transformers and hybrid models and might sometimes bring good performance for ConvNets, adopting BN after each stage in pure convolution models still yields better performance. Moreover, we replace BN with precise BN [129] (pBN), which is an optimal alternative normalization strategy to BN. We find slight performance improvements (around 0.1%), especially when MogaNet-S/B adopts the EMA strategy (by default), indicating that we can further improve MogaNet with advanced BN. As discussed in ConvNeXt, EMA might severely hurt the performances of models with BN. This phenomenon might be caused by the unstable and inaccurate BN statistics estimated by EMA in the vanilla BN with large models, which will deteriorate when using another EMA of model parameters. We solve this dilemma by exponentially increasing the EMA decay from 0.9 to 0.9999 during training as momentum-based contrastive learning methods [6, 12], *e.g.*, BYOL [35]. It can also be tackled by advanced BN variants [48, 129].

Norm (after)	Input size	LN	LN	BN	pBN
Norm (within)	size	LN	BN	BN	pBN
MogaNet-T	224^2	78.4	79.1	79.0	79.1
MogaNet-T	256^2	78.8	79.4	79.6	79.6
MogaNet-S (EMA)	224^2	82.7	83.3	83.4	83.5
MogaNet-B (EMA)	224^2	83.6	84.1	84.2	84.3

Table A5. Ablation of normalization layers used in MogaNet.

C.4. Refined Training Settings for Lightweight Models

To explore the full power of lightweight models of our MogaNet, we refined the basic training settings for MogaNet-XT/T according to RSB A2 [122] and DeiT-III [109]. Compared to the default setting as provided in Table A2, we only adjust the learning rate and the augmentation strategies for faster convergence while keeping other settings unchanged. As shown in Table A6, MogaNet-XT/T gain +0.4~0.6% when use the large learning rate of 2×10^{-3} and 3-Augment [109] without complex designs. Based on the advanced setting, MogaNet with 224^2

input resolutions yields significant performance improvements against previous methods, *e.g.*, MogaNet-T gains +3.5% over DeiT-T [106] and +1.2% over Parc-Net-S [145]. Especially, MogaNet-T with 256^2 resolutions achieves top-1 accuracy of 80.0%, outperforming DeiT-S of 79.8% reported in the original paper, while MogaNet-XT with 224^2 resolutions outperforms DeiT-T under the refined training scheme by 1.2% with only 3M parameters.

Model	Input size	Learning rate	Warmup epochs	Rand Augment	3-Augment [109]	EMA	Top-1 Acc (%)
DeiT-T [106]	224^2	1×10^{-3}	5	9/0.5	×	✓	72.2
DeiT-T [106]	224^2	2×10^{-3}	20	×	✓	×	75.9
ParC-Net-S [145]	256^2	1×10^{-3}	5	9/0.5	×	✓	78.6
ParC-Net-S [145]	256^2	2×10^{-3}	20	×	✓	×	78.8
MogaNet-XT	224^2	1×10^{-3}	5	7/0.5	×	×	76.5
MogaNet-XT	224^2	2×10^{-3}	20	×	✓	×	77.1
MogaNet-T	224^2	1×10^{-3}	5	7/0.5	×	×	79.0
MogaNet-T	224^2	2×10^{-3}	20	×	✓	×	79.4
MogaNet-T	256^2	1×10^{-3}	5	7/0.5	×	×	79.6
MogaNet-T	256^2	2×10^{-3}	20	×	✓	×	80.0

Table A6. Advanced training recipes for Lightweight models of MogaNet on ImageNet-1K.

D. More Comparison Experiments

In addition to Sec. 5.1, we further provide comparison results for 100 and 300 epochs training on ImageNet-1K. As for 100-epoch training, we adopt the original RSB A3 [122] setting for all methods, which adopts LAMB [137] optimizer and a small training resolution of 160^2 . As for 300-epoch training, we report results of RSB A2 [122] for classical CNN or the original setting for Transformers or modern ConvNets. In Table A7, when compared with models of similar parameter size, our proposed MogaNet-XT/T/S/B achieves the best performance in both 100 and 300 epochs training. Results of 100-epoch training show that MogaNet has a faster convergence speed than previous architectures. For example, MogaNet-T outperforms EfficientNet-B0 and DeiT-T by 1.3% and 7.6%, MogaNet-S outperforms Swin-T and ConvNeXt-T by 4.1% and 1.6%, MogaNet-B outperforms Swin-S and ConvNeXt-S by 2.5% and 1.0%.

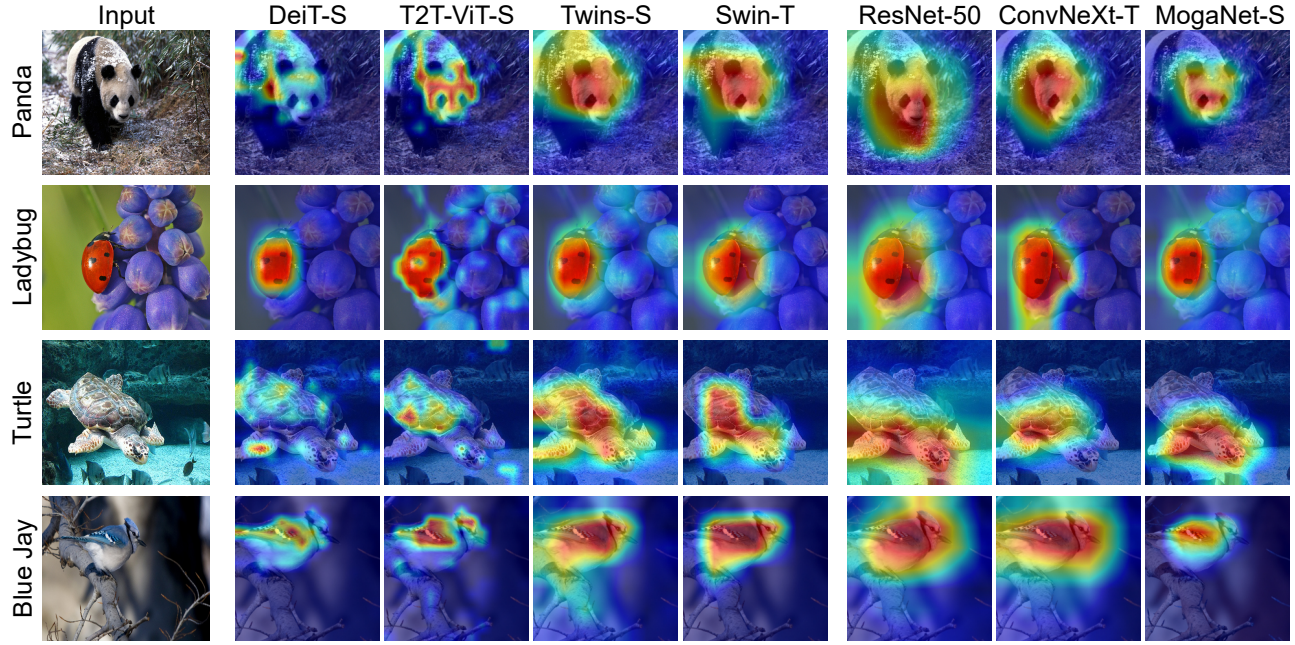


Figure A2. Visualization of Grad-CAM activation maps of the models trained on ImageNet-1K.

Architecture	Data	Param. (M)	100-epoch			300-epoch		
			Train	Test	Acc (%)	Train	Test	Acc (%)
ResNet-18 [42]	CVPR'2016	12	160	224	68.2	224	224	70.6
ResNet-34 [42]	CVPR'2016	22	160	224	73.0	224	224	75.5
ResNet-50 [42]	CVPR'2016	50	160	224	78.1	224	224	79.8
ResNet-101 [42]	CVPR'2016	45	160	224	79.8	224	224	81.3
ResNeXt-50 [132]	CVPR'2017	25	160	224	79.2	224	224	80.4
SE-ResNet-50 [51]	CVPR'2018	28	160	224	77.0	224	224	80.1
EfficientNet-B0 [103]	ICML'2019	5	160	224	73.0	224	224	77.1
EfficientNet-B1 [103]	ICML'2019	8	160	224	74.9	240	240	79.4
EfficientNet-B2 [103]	ICML'2019	9	192	256	77.5	260	260	80.1
EfficientNet-B3 [103]	ICML'2019	12	224	288	79.2	300	300	81.4
EfficientNet-B4 [103]	ICML'2019	19	320	380	81.2	380	380	82.4
RegNetY-800MF [90]	CVPR'2020	6	160	224	73.8	224	224	76.3
RegNetY-4GF [90]	CVPR'2020	21	160	224	79.0	224	224	79.4
RegNetY-8GF [90]	CVPR'2020	39	160	224	81.1	224	224	79.9
RegNetY-16GF [90]	CVPR'2020	84	160	224	81.7	224	224	80.4
EfficientNetV2-rw-S [104]	ICML'2021	24	224	288	80.9	288	384	82.9
EfficientNetV2-rw-M [104]	ICML'2021	53	256	384	82.3	320	384	81.9
DeiT-T [106]	ICML'2021	6	160	224	66.7	224	224	72.2
DeiT-S [106]	ICML'2021	22	160	224	73.8	224	224	79.8
DeiT-B [106]	ICML'2021	87	160	224	76.0	224	224	81.8
Swin-T [73]	ICCV'2021	28	160	224	77.0	224	224	81.3
Swin-S [73]	ICCV'2021	50	160	224	79.7	224	224	83.0
ConvNeXt-T [74]	CVPR'2022	29	160	224	79.5	224	224	82.1
ConvNeXt-S [74]	CVPR'2022	50	160	224	81.2	224	224	83.1
VAN-B0 [37]	arXiv'2022	4	160	224	72.6	224	224	75.8
VAN-B2 [37]	arXiv'2022	27	160	224	81.0	224	224	82.8
VAN-B3 [37]	arXiv'2022	45	160	224	81.9	224	224	83.9
MogaNet-XT	Ours	3	160	224	72.8	224	224	76.5
MogaNet-T	Ours	5	160	224	74.3	224	224	79.0
MogaNet-S	Ours	25	160	224	81.1	224	224	83.4
MogaNet-B	Ours	44	160	224	82.2	224	224	84.2

Table A7. ImageNet-1K classification performance of tiny to medium size models (5~50M) training 100 and 300 epochs. RSB A3 [122] setting is used for 100-epoch training of all methods. As for 300-epoch results, the RSB A2 [122] setting is used for ResNet, ResNeXt, SE-ResNet, EfficientNet, and EfficientNetV2, while other methods adopt settings in their original paper.